Cellular and Molecular Life Sciences (2023) 80:226
https://doi.org/10.1007/s00018-023-04868-8

ORIGINAL ARTICLE

Restored UBE2C expression in islets promotes β-cell regeneration in mice by ubiquitinating PER1

Hemin Jiang[1] · Shuai Zheng[1] · Yu Qian[1] · Yuncai Zhou[1] · Hao Dai[1] · Yucheng Liang[1] · Yunqiang He[1] · Rui Gao[1] · Hui Lv[1] · Jie Zhang[1] · Zhiqing Xia[1] · Wenxuan Bian[1] · Tao Yang[1] · Qi Fu[1]

Received: 16 January 2023 / Revised: 8 July 2023 / Accepted: 10 July 2023 / Published online: 24 July 2023

Abstract

Insulin deficiency may be due to the reduced proliferation capacity of islet β-cell, contributing to the onset of diabetes. It is therefore imperative to investigate the mechanism of the β-cell regeneration in the islets. NKX6.1, one of the critical β-cell transcription factors, is a pivotal element in β-cell proliferation. The ubiquitin-binding enzyme 2C (UBE2C) was previously reported as one of the downstream molecules of NKX6.1 though the exact function and mechanism of UBE2C in β-cell remain to be elucidated. Here, we determined a subpopulation of islet β-cells highly expressing UBE2C, which proliferate actively. We also discovered that β-cell compensatory proliferation was induced by UBE2C via the cell cycle renewal pathway in weaning and high-fat diet (HFD)-fed mice. Moreover, the reduction of β-cell proliferation led to insulin deficiency in β*Ube2c*KO mice and, therefore, developed type 2 diabetes. UBE2C was found to regulate PER1 degradation through the ubiquitin–proteasome pathway via its association with a ubiquitin ligase, CUL1. PER1 inhibition rescues UBE2C knockout-induced β-cell growth inhibition both in vivo and in vitro. Notably, overexpression of UBE2C via lentiviral transduction in pancreatic islets was able to relaunch β-cell proliferation in STZ-induced diabetic mice and therefore partially alleviated hyperglycaemia and glucose intolerance. This study indicates that UBE2C positively regulates β-cell proliferation by promoting ubiquitination and degradation of the biological clock suppressor PER1. The beneficial effect of UBE2C on islet β-cell regeneration suggests a promising application in treating diabetic patients with β-cell deficiency.

Hemin Jiang, Shuai Zheng, Yu Qian and Yuncai Zhou are contribute equally to this work and share co-first authorship.

✉ Tao Yang
yangt@njmu.edu.cn

✉ Qi Fu
drfuqi@njmu.edu.cn

[1] Department of Endocrinology, The First Affiliated Hospital of Nanjing Medical University, Nanjing, China

Graphical abstract

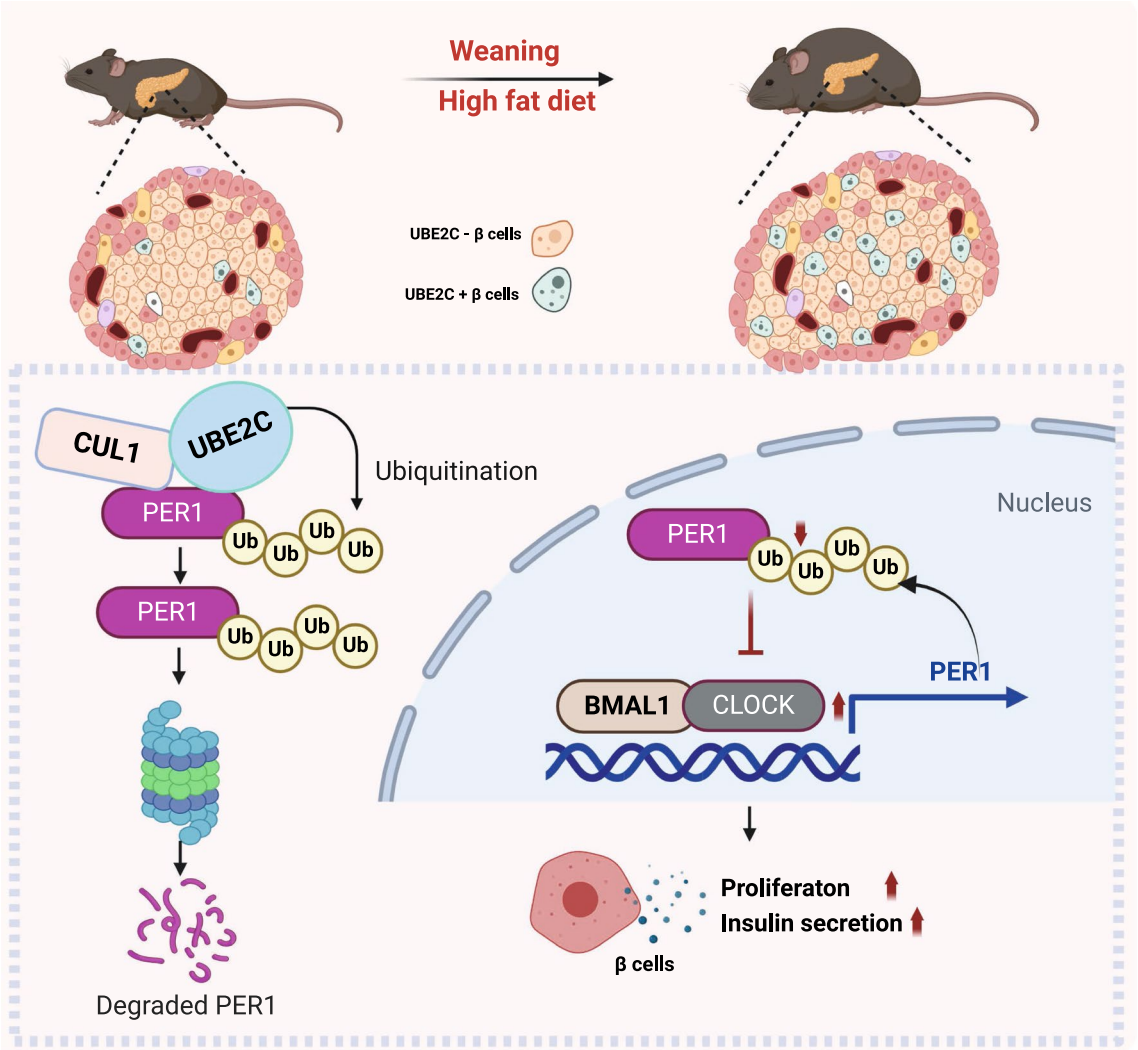

Keywords UBE2C · β-cell regeneration · Ubiquitination · PER1

Introduction

Diabetes is characterized by hyperglycaemia caused by a relative or absolute low level of insulin [1, 2]. As a unique source of insulin, islet β-cells are either insufficient or vanished [3–5]. C-peptide, which protects kidney function, [6, 7] and hepatic glucose output inhibitory non-coding RNA are both produced from β-cells [8, 9], indicating an important role of β-cells in preventing diabetes progression. Therefore, protecting and promoting β-cell regeneration is more beneficial than traditional treatments such as insulin injection.

A lineage-tracing assay using β-cell-specific fluorescent mice showed that replication is the primary mode of β-cell regeneration [10]. Islet β-cells proliferate explosively during infancy and early childhood but gradually decline associated with the maturation of insulin secretory machinery. However, certain pathophysiological conditions, including obesity and pregnancy, can boost β-cell proliferation [11–13]. A major cause of type 2 diabetes is an unhealthy lifestyle, especially a high-fat diet, which causes the high incidence of type 2 diabetes in many countries [14, 15]. According to the previous reports, the patients developing type 2 diabetes are a group of people who cannot

compensate for increasing insulin requirement in the body, and the main cause of this problem is the decline of islet β-cell proliferative capacity [16]. Exploring the mechanism of β-cell compensatory replication would provide key insights into β-cell regeneration and treatment of type 2 diabetes.β-cells show significant heterogeneity in islets for their spatial distribution and maturation stages [17]. In the present study, single-cell RNA sequencing (scRNA-seq) was introduced to define different subgroups of islet β-cells, and scRNA-seq was also performed on high-fat diet (HFD)-induced obese mouse islets. A β-cell subgroup with high replication capacity was identified, and ubiquitin-binding enzyme 2C (UBE2C) was a top three characteristic gene of this group of cells. UBE2C is an important member of the ubiquitin-conjugating enzymes (E2) family, and its overexpression promotes proliferation and inhibits apoptosis of tumour cells [18, 19]. Although UBE2C has been reported as one of the downstream molecules of NKX6.1, a critical transcription factor regulating β-cell proliferation [20], the exact function and mechanism of UBE2C in pancreatic islets remain unknown.

To investigate the regulatory mechanism of UBE2C in β-cell replication, β-cell-specific UBE2C conditional knockout (β*Ube2c*KO) mice were generated. β*Ube2c*KO mice developed hyperglycaemia due to β-cell deficiency-induced insulin insufficiency. Using immunoprecipitation and mass spectrometry (MS), the core protein of the SCF E3 ubiquitin ligase complex, CUL1, was confirmed to associate with UBE2C. Moreover, the negative regulator of cellular circadian rhythm PER1 was found as the target of the UBE2C/CUL1 complex. The complex promoted the degradation of PER1 and then stimulated the proliferation of β-cells through cell cycle reinitiation. Our investigation revealed a previously unexplored role of UBE2C in β-cell regeneration both in vitro and in vivo and demonstrated the effectiveness of introducing UBE2C to treat STZ-induced diabetic mice.

Materials and methods

Animal experiments

Animal use procedures were approved (IACUC1804001) by the Medicine Animal Care Committee of Nanjing Medical University. Experiments were conducted in accordance with relevant institutional guidelines and regulations.

C57BL/6J and *Ube2c*$^{fl/fl}$ mice were purchased from the Model Animal Research Center of Nanjing University. *Ins1*-Cre mice were obtained from Jackson Laboratory. To produce β-cell-specific knockout mice, *Ube2c*$^{fl/fl}$ mice were hybridized with MIP-Cre mice. In this study, mice with INS1-specific deletion of UBE2C were defined as β*Ube2c*KO mice and *Ube2c*$^{fl/fl}$ mice were used as controls. The genotype of the mice was analysed through polymerase chain reaction (PCR) using mouse tail genomic DNA, and Western blotting (WB) was used for verification at the protein level (Supplementary Fig. 2). Male β*Ube2c*KO mice, *Ube2c*$^{fl/fl}$ mice, and C57BL/6 J mice were maintained at 22 °C on a 12-h light–dark cycle with ad libitum access to a normal chow diet (CD, 13.5% fat; LabDiet 5001) or HFD (60% fat; Research Diets D12492). Body weights were monitored periodically.

Tests for glucose and insulin

Mice were subjected to an intraperitoneal glucose tolerance test (IPGTT) and insulin tolerance tests (ITT) using established protocols [21]. Briefly, mice were fasted for 16 h or 5 h at intervals of 4 weeks before the IPGTTs and ITT experiment. D-glucose (2 g/kg) for the IPGTT or insulin (0.75 U/kg; Humulin R; Eli Lilly, Indianapolis, IN, USA) for the ITT was delivered by I.P. injection. Blood glucose level and whole blood insulin level from the tail vein were monitored at 0, 15, 30, 60, and 120 min.

Virus infusion within pancreatic ducts

Male C57BL/6J mice treated with STZ were injected with pSLenti-SFH-EGFP-P2A-Puro-CMV-Ube2c-3xFLAG-WPRE (LV-UBE2C) or pSLenti-SFH-EGFP-P2A-Puro-CMV-MCS-3xFLAG-WPRE (Vector) (OBIO Technology). Male β*Ube2c*KO mice and *Ube2c*$^{fl/fl}$ mice after 4 weeks HFD feeding were injected with pAV-4in1shRNA (control)-CMV-GFP (shCTR) or pAV-4in1shRNA (PER1)-CMV-GFP (shPER1) (WZ Biosciences). For the pancreatic ductal infusion, mice were anaesthetized via inhalation of isoflurane. A total volume of 150 viral solutions were infused through the pancreatic/biliary duct at a rate of 6 μL/min with a clip placed on the bile duct to avoid the perifusion of hepatic duct [22].

Islet isolation and hormone secretion assay

Isolation and culture of islets, islet/β-cell line glucose-stimulated insulin secretion (GSIS) assay, and islet perifusion were performed as previously described [21]. For GSIS, a total of 30 islets or β-cell lines were seeded in a 48-well plate and incubated with glucose free Kreb's buffer for 30 min, before treatment with 2 mM or 20 mM glucose for 1 h.

Mice islets were isolated as follows: The entrance to the duodenum was clamped with a haemostat and 0.5 mg/ml collagenase P in cold Hanks' balanced salt solution (HBSS; Roche Diagnostics, Mannheim, Germany) was injected into the bile duct. The expanded mouse pancreatic tissue was digested at 37 °C for 14 min 30 s and then filtered using a 600-μm mesh. Cold HBSS with 10% foetal bovine serum

(FBS) was added to stop the reaction. A gradient comprising layers of HBSS and Histopaque-11191 (Sigma Aldrich) was used to separate the islets, which were then manually selected two times. The islets were then dispersed into single cells using TrypLE (Thermo Scientific) for 15 min in a 37 °C water bath and then resuspended in Dulbecco phosphate-buffered saline with 2% FBS.

Primary islets were cultured overnight before the perifusion assay. 120 islets were placed into the perifusion chambers and firstly treated with Kreb's buffer containing 0 mM glucose for 40 min, followed by Kreb's buffers containing 20 mM glucose for 30 min, at the rate of 1 ml/min. Fractions were collected every minute, starting from the 30th minute. Secreted insulin were normalized to total DNA content of islets recollected from the chambers. Levels of insulin (Mercodia), glucagon (Mercodia), and somatostatin (Phoenix Pharmaceuticals) were measured using enzyme-linked immunosorbent assay (ELISA) kits, according to the manufacturer's instructions.

Pancreatic insulin concentration

Mice were weighed and extracted for pancreas after 16 h fasting. After weighed for insulin content correction, pancreas was put into the tissue grinding tube with 1 ml acid-alcohol (75% ethanol, 0.15 mol/l HCL). Pancreatic homogenate was extracted overnight at 4 °C after grinding by tissue grinder. On the second day, tubes were centrifuged for 10 min at 3500r/min in 4 °C. After the collection of supernatants (store at − 80 °C), equal volume of acid-alcohol (75% ethanol, 0.15 mol/l HCL) was added into the tissue grinding tube. The extraction was repeated for 4–5 times. Insulin in total supernatants was determined by Elisa kits (Mercodia) following the manufacturer's instructions.

Transmission electron microscopy (TEM)

Islets were fixed in 2.5% glutaraldehyde and 2.5% paraformaldehyde in cacodylate buffer (0.1 M, pH 7.4), post-fixed in osmium tetroxide, dehydrated in graded series of alcohol, and finally embedded in EPON 812. Ultrathin sections (60 − 80 nm) of selected regions were obtained with a diamond knife. Tecnai™ G2 Spirit BioTwin (FEI, Hillsboro, OR, USA) with an accelerating voltage of 80 kV was used to examine the samples [21]. Mature insulin granules were quantified using grayscale threshold analyses. The immature and docked granules were counted manually. Granules located within 100 nm of the plasma membrane without signs of fusion were considered "docked".

Immunofluorescence staining

Pancreatic tissue was fixed in formalin, incubated in ethanol and xylene, and embedded in paraffin. It was sliced into 5-μm sections, dewaxed in xylene, and rehydrated using a graded series of alcohol solutions. The sections were subjected to antigen retrieval and blocked with serum. Sections were incubated with primary antibodies overnight in the dark at 4 °C. The antibodies used in this study are listed in Supplementary Table 1. After rewarming to room temperature and washing, sections were incubated with secondary antibodies for 2 h in the dark at room temperature. Images were acquired using a fluorescence microscope (Zeiss).

Cell culture

The mouse β-cell line, MIN6, was a kind gift from Professor Zhuoxian Meng (Zhejiang University Medical College). Cells were cultured in Dulbecco's modified Eagle's medium (DMEM; Invitrogen, Carlsbad, CA, USA) (25 mM glucose) containing 15% foetal bovine serum (FBS; Gibco), HEPES (10 mmol/L), sodium pyruvate (1 mmol/L), penicillin (100 U/mL), streptavidin (100 μg/mL), and β-mercaptoethanol (50 μmol/L).

The mouse β-cell line, βTC-6, was purchased from the Cell Bank of the Chinese Academy of Sciences (Kunming, China) and cultured in DMEM (25 mM glucose) containing 10% FBS, penicillin (100 U/mL), streptavidin (100 μg/mL), and β-mercaptoethanol (50 μmol/L).

The human embryonic kidney cell line, 293 T, was purchased from the Cell Bank of the Chinese Academy of Sciences (Shanghai, China) and cultured in DMEM containing 10% FBS, penicillin (100 U/mL), and streptavidin (100 μg/mL).

Co-immunoprecipitation

The cells were lysed in lysis buffer. After centrifugation, 10% of the supernatant was used as input, and the remainder was immunoprecipitated with agarose A/G beads (Roche), immunoglobulin G (IgG, negative controls), or with antibodies for the target proteins overnight at 4 °C. Pellets were washed thrice with wash buffer, resuspended in sodium dodecyl sulphate (SDS, 2 × concentration), and subjected to Western blotting (WB).

Western blotting

Cell lysates were prepared using RIPA lysis buffer on ice. The protein concentration was measured using the bicinchoninic acid (BCA) Assay Kit (Beyotime). WB was performed using the indicated antibodies (Supplementary

Table 2). Protein blots were visualized using SuperSignal West Pico Chemiluminescent Substrate (Pierce Biotechnology) in a ChemiDoc XRS + system (Bio-Rad Laboratories).

Mass spectrometry analysis

MS was performed on the precipitated protein using co-immunoprecipitation with UBE2C antibody of βTC-6 cells transfected with lentivirus-UBE2C or empty vectors. Through the use of a nanospray source, the labelled peptides were analysed on the LTQ-Orbitrap instrument (Thermo Fisher). LC–MS/MS was operated in positive ion mode, with a linear gradient from 0 to 60% of buffer B (CH3CN) in 150 min and a flow rate of 200 nl/min. Five MS/MS scans were conducted on each of the five highest peaks from βTC-6 cells for the analysis of proteins. MS/MS spectra of precursor ions were submitted to Maxquant (version 1.2.2.5) using the search parameters as previously described [23].

Tandem mass tag (TMT) quantification proteomics

TMT-labelled quantitative proteomics was performed on the total extracted protein of βTC-6 cells transfected with lentivirus-UBE2C or empty vectors using the TMT strategy, as previously described [24]. Briefly, the samples were dissolved in lysate buffer consisting of 1% protease inhibitor, 8 M urea, 50 mM NAM, and 3 μM TSA.

After measuring protein concentration, protein samples were treated with 5 mM DTT for 30 min at 56 °C, followed by 11 mM iodoacetamide for 15 min at room temperature in the dark. After trypsin digestion overnight, Strata X C18 SPE column was used to desalt the peptides overnight, followed by vacuum drying, reconstituted with 0.5 M TEAB, and labelled with TMT kit. For liquid chromatography (LC)–tandem mass spectrometry (MS) analysis, tryptic peptides were dissolved in liquid phase A (0.1% formic acid) loaded on a reversed-phase analytical column and separated with the EASY-nLC 1200 ultra-performance LC system (Thermo Fisher Scientific). The gradient of liquid phase B (90% acetonitrile containing 0.1% formic acid) was set as 0–40 min at 6–22%, 40–54 min at 22–32%, 54–57 min at 32–80%, or 57–60 min at 80% with 500 nL/min flow rate. The peptides were then subjected to tandem MS using Q Exactive (Thermo Fisher Scientific). Detection was conducted using an Orbitrap ion trap mass analyser (Thermo Fisher Scientific) at 2.1 kV. The primary MS system scanned from 350 to 1600 m/z, while the secondary tandem MS system scanned a startup of 100 m/z. A data-dependent procedure was used with 30 s of dynamic exclusion. The automatic gain control was set to 1E5. MaxQuant software was used to retrieve MS2 data. Significantly differentially expressed proteins were screened at $P < 0.05$ and a fold change of > 1.2 or < 0.83.

siRNA and plasmid transfection

MIN6 or βTC-6 cells were seeded in six-well plates and 24-well plates and cultured until they reached 70% confluence. Transient transfection with siRNA or plasmids was done using Lipo3000 (Life Technologies, Carlsbad, CA, USA). The siRNA sequences are listed in Supplementary Table 3. All assays were performed 48 h after transfection.

Quantitative real-time PCR (qRT-PCR)

Total RNA was extracted from tissues and cells using TRIzol reagent (Life Technologies).

For each sample, RNA was reverse transcribed using PrimeScript™ RT reagent kit (Takara Bio, Kusatsu, Japan). qRT-PCR was performed with SYBR Green PCR Master Mix (Takara Biotechnology) and analysed using a real-time PCR system (Roche), as previously described [21]. The primer sequences used are listed in Supplementary Table 4. The relative gene expression was calculated using the comparative CT ($2-\Delta\Delta$CT) method with β-actin as a reference gene.

Bulk RNA-seq

Islets for RNA-seq were collected from the β*Ube2c*KO and control mice. RNA-seq methods have been previously described [25]. Briefly, TRIzol reagent (Invitrogen, CA, USA) was used to isolate total RNA from handpicked islets according to the manufacturer's instructions. On-chip electrophoresis was used to measure the quality and quantity of extracted RNA using the Agilent RNA 6000 Nano Kit and Agilent 2100 Bioanalyzer (Agilent Technologies, CA, USA). Library preparation was performed on samples exhibited $1.9 \le$ A260/A280 ≤ 2.2, RNA integrity number > 8.0, and 28S/18S > 1.0. By enriching poly (A) mRNA with magnetic oligo (dT) beads, total RNA was purified. With the random hexamer (N6) primers, double-stranded cDNA fragments were synthesized and subjected to end repair and adapter ligation. As a next step, PCR amplification was used to construct cDNA libraries, which were then sequenced on BGISEQ-500 by Beijing Genomics Institute (Shenzhen, China). Gene expression was quantified using RSEM 1.1.12 software and normalized using the method of fragments per kilobase of exon model per million reads mapped (FPKM). DEseq2 (fold change ≥ 2 and $p_{\text{adjusted}} \le 0{\cdot}05$) was used to identify differentially expressed genes (DEGs) between the β*Ube2c*KO and control groups.

Single-cell (sc)RNA-seq and datasets analysis

Islet cells from HFD and CD mice were dispersed into single cells and subjected to scRNA-seq, and the reads were processed as our previous study described [26]. scRNA-seq was performed by Shanghai Biotechnology Corporation. The single cells were used to create gel beads in emulsion (GEM) utilizing a Chromium™ Single Cell Platform (10 × Genomics) with a Chromium™ Single Cell 3′ GEM, Library & Gel Bead Kit v3 and a Chromium™ Chip B Single Cell Kit, according to the manufacturer's guidelines. The beads were then placed in a single tube and underwent reverse transcription; each cDNA was tagged at the 5′ end with a unique molecular identifier (UMI) and a label indicating the cell of origin (according to the manufacturer's standard guidelines [CG000206 Rev D]). The libraries were quantified on a 2100 Bioanalyzer (Agilent) using a High Sensitivity DNA Chip (Agilent) and a Qubit High Sensitivity DNA Assay Kit (Thermo Fisher Scientific). Lastly, a NovaSeq 6000 system (2 × 150 bp read lengths; Illumina) was used to conduct sequencing. The data were scaled and principal component analysis (PCA) was based on the top 2000 high variable genes. The top 20 principles were used for t-distributed stochastic neighbour embedding (t-SNE) and uniform manifold approximation and projection (UMAP) construction [27]. Using the Louvain method, the unsupervised cell cluster result was based on the top 20 principal components acquired using PCA [28]. We assigned β-cell types according to the expression of the marker gene Ins1. For the sub-clustering of β-cells, we applied the same scaling, dimensionality reduction, and clustering procedures. We identified significant DEGs among the β-cell subpopulations using the Wilcoxon rank-sum test. The DEGs were subjected to Kyoto Encyclopedia of Genes and Genomes (KEGG) enrichment analysis.

Cell proliferation assay

Cell number was determined using the Cell Counting Kit (CCK)-8 assay (Beyotime). Percent cell proliferation was detected using the 5-ethynyl-2′-deoxyuridine (EdU) assay (RiboBio). The ratio of cells positive for EdU to cells positive for 4′,6-diamidino-2-phenylindole (DAPI) was used to denote the percentage of EdU-positive cells. The cell cycle was detected using propidium iodide (PI) staining (Millipore Sigma).

Beta cell mass calculation

Images from 4 to 6 insulin-stained pancreas sections per mouse with each section separated by at least 250 μm were measured using ImageJ software to determine beta cell area. Then, the beta cell mass was calculated by multiplying the average percentage of beta cell area by the pancreas weight of corresponding mice.

Statistical analyses

The immunostaining of mouse pancreas sections was analysed using ImageJ software. Immunofluorescence microscopy was used to assess Ki67 + β-cell proliferation. DAPI-stained insulin-positive cells were considered β-cells. DAPI + and Ki67 + insulin-positive cells were considered proliferative β-cells. β-cell proliferation index from each mouse was calculated based on the ratio of the number of Ins and Ki67 double-positive cells over the number of whole INS + cells with DAPI staining. Sections were viewed with 10 × objective, and all beta cells on the entire section were counted (1000–3000 β-cells per section for non-diabetic mice). As beta cells were reduced after STZ treatment, more than 15 islets (over 1000 β-cells) in three pancreatic sections were analysed per STZ-treated mouse. Data comparisons between the two groups were performed using two-tailed *t*-tests or analysis of variance (ANOVA) with Tukey's test which corrects for multiple hypotheses. AUC was calculated by trapezoid analysis and was compared by *t*-test. Data are the mean ± SD. Statistical significance was set at $P < 0.05$. Graphs and statistical analyses were completed using GraphPad Prism 8.0 (GraphPad Software, San Diego, CA, USA).

Results

ScRNA-seq data showed *Ube2c* was highly expressed in human and murine proliferating β-cells

C57BL/6 J mice were fed an HFD for 8 weeks, which was reported to induce the compensatory proliferation of islet β-cells [21]. To get an expression profile of these actively proliferating β-cells, we performed scRNA-seq to characterize them. Islet cells from HFD- and CD-fed mice were annotated based on the expression of the predominant hormone gene, Ins1, resulting in 14,108 β-cells and then clustered into nine clusters using UMAP according to our previous study [29] (Fig. 1A). The cell cycle analysis indicated that β-cells in Cluster-7 were in the G2M phase, whereas the other clusters were in the G1 and S phases (Fig. 1B). We, therefore, would like to define Cluster-7 by specific gene expression profile and found that *Ube2c* was rich-expressed gene in Cluster-7, while it was barely expressed in other clusters (Fig. 1C). With the finding above, we determined the cells in Cluster-7 as *Ube2c*^{high} β-cells and the others were defined as *Ube2c*^{low} β-cells (Fig. 1D). The genes engaging in "DNA replication", "cell cycle", and "ubiquitin-mediated proteolysis pathways" were highly expressed in *Ube2c*^{high} β-cells by

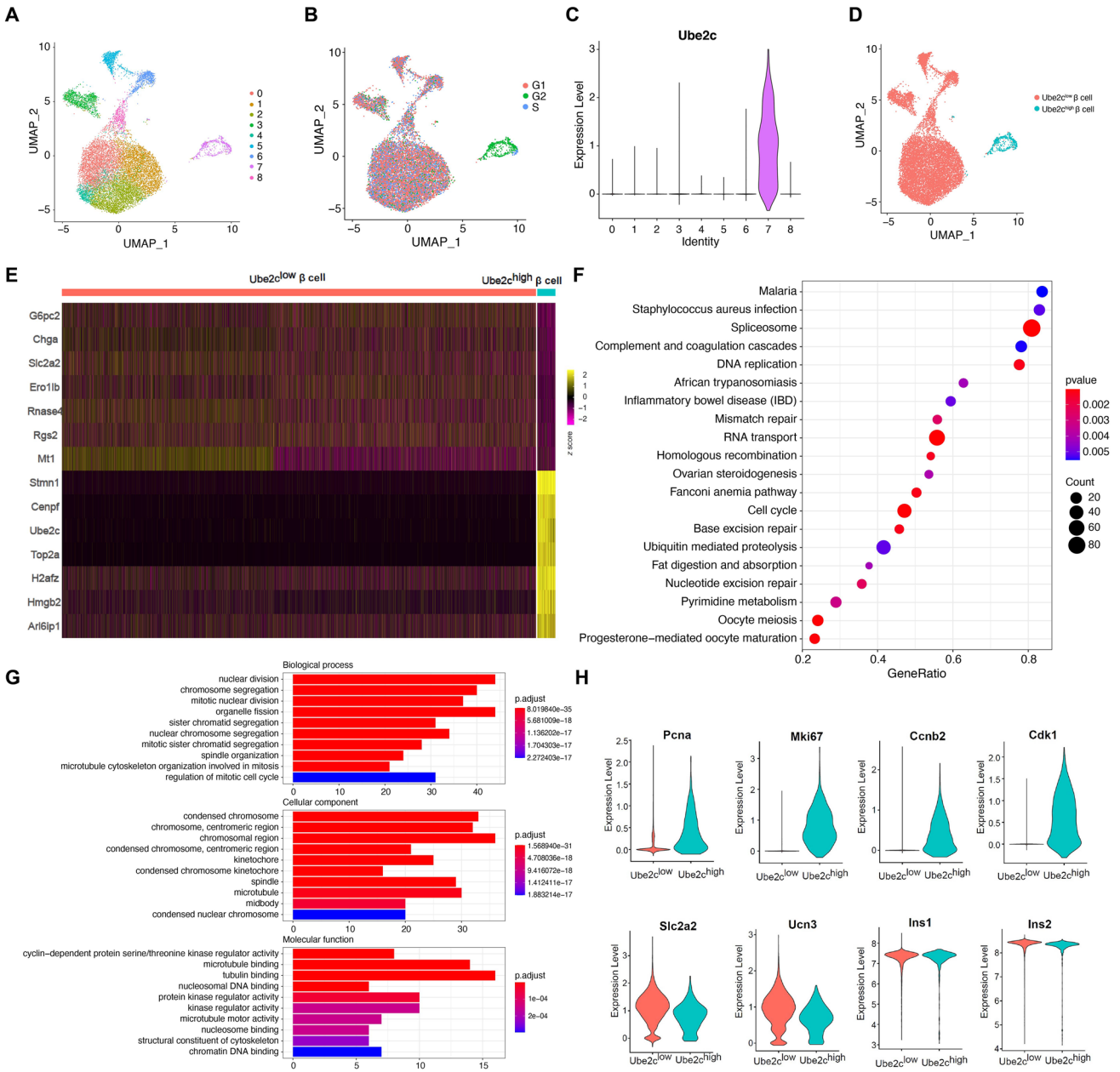

Fig. 1 Heterogeneous expression of *Ube2c* on the islet β-cells of mice. **A** Visualization of β-cell clustering using uniform manifold approximation and projection (UMAP) maps; **B** UMAP map showing cell cycle distribution; **C** Violin map showing *Ube2c* expression distribution in each β-cell subpopulation; **D** UMAP map showing *Ube2c*^{high} and *Ube2c*^{low} subpopulations in β-cells. **E** Heatmap of differentially expressed genes (DEGs) in *Ube2c*^{low} and *Ube2c*^{high} subgroups. **F** GSEA pathway enrichment map showing *Ube2c*^{high} β-cell subpopulations. **G** DEGs between *Ube2c*^{high} and *Ube2c*^{low} subpopulation of β-cell based on the GO database. **H** Violin plots of cell cycle- and β-cell function-related genes expressed in *Ube2c*^{low} and *Ube2c*^{high} subpopulations. Expression of *Pcna*, *Ki67*, *Ccnb2*, and *Cdk1* was upregulated markedly in *Ube2c*^{high} β-cells, expression of *Slc2a2* and *Ucn3* was upregulated slightly in *Ube2c*^{low} β-cells, and there was no difference in expression of *Ins1* or *Ins2*

Gene set enrichment analysis (GSEA) (Fig. 1F). Differentially expressed genes (DEGs) were examined through Gene Ontology (GO) enrichment analysis, which revealed that the genes involved in "mitosis", "chromosome segregation", and "cell cycle-dependent serine/threonine kinase activity" were expressed on a different level in *Ube2c*^{high} and *Ube2c*^{low} β-cells (Fig. 1G).

Compared to the *Ube2c*^{low} subpopulation, genes related to cell proliferation and cell cycle, such as *Pcna*, *Mki67, Ccnb2*, and *Cdk1*, were highly expressed in *Ube2c*^{high} subpopulation. Contrary to the phenomenon written above, the

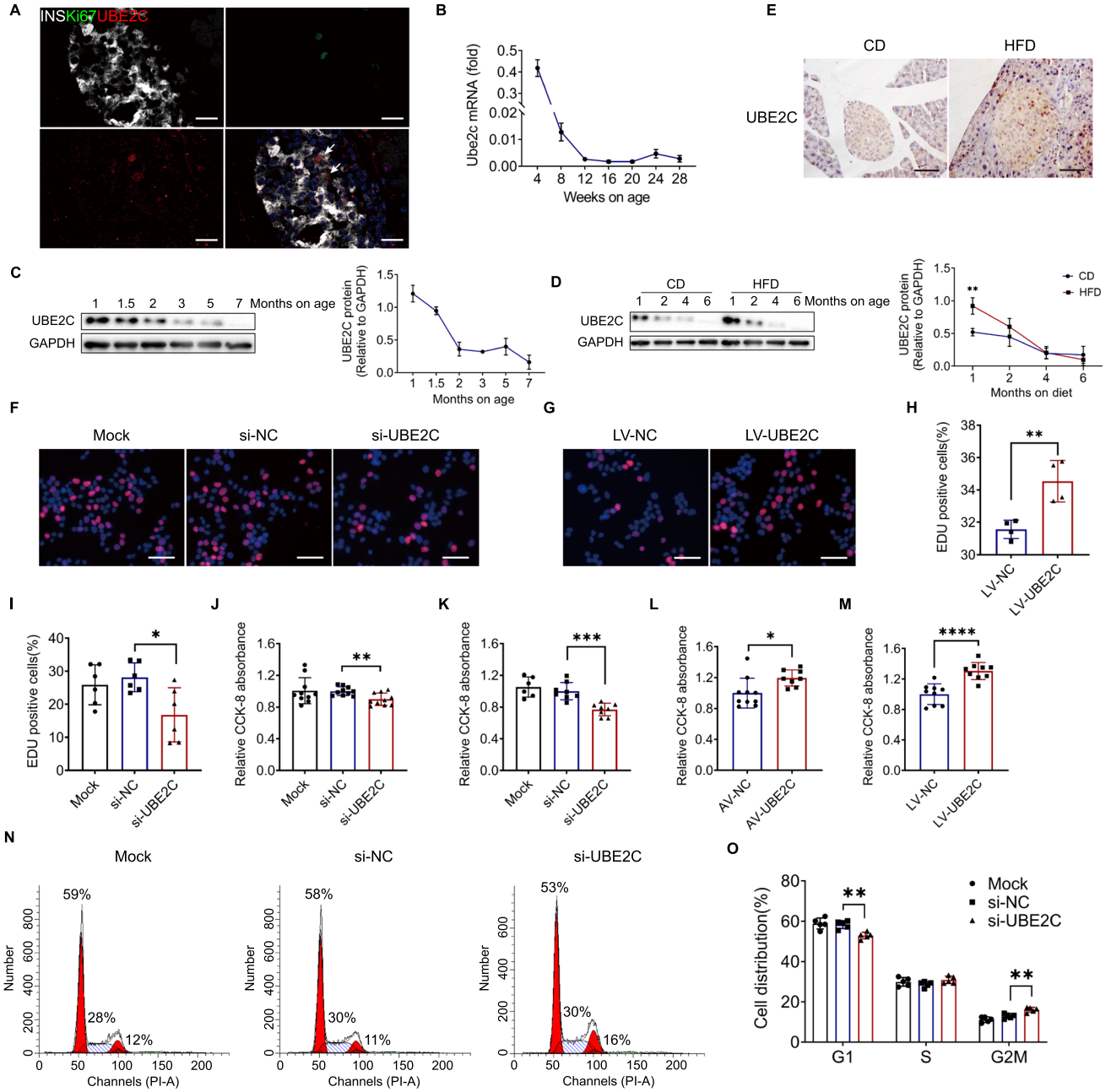

Fig. 2 High expression of UBE2C promotes the proliferation of islet β-cells. **A** Representative images of insulin (white), Ki67 (green), UBE2C (red), and DAPI (blue) immunostaining in the pancreas of 4-week-old C57BL/6J mice. Scale bar: 20 μm. **B** and **C** Islets of chow-fed C57BL/6J mice 1, 1.5, 2, 3, 5, and 7 months after birth were extracted. (B) RT-qPCR for measurement of expression of *Ube2c* mRNA, (C) Western blotting to measure protein expression of UBE2C. Band density was measured and normalized to GAPDH (N = 4–6 mice/group). **D** C57BL/6 J male mice were fed with normal chow diet (CD) or high-fat diet (HFD) from 4 weeks of age; then islets were extracted at 1, 2, 4, and 6 months of feeding, and expression of UBE2C protein was measured in CD and HFD groups using Western blotting, normalized to GAPDH, and represented graphically at the right of each panel. ($N = 3$ mice/group). **E** Pancreatic sections of C57BL/6J mice after 4 weeks of HFD or CD feeding were assessed through immunohistochemistry using the UBE2C antibody. Scale bar: 40 μm. **F** and **I** Cell proliferation was assessed using the EdU assay 72 h after si-UBE2C transfection of βTC-6 cells. ($N = 4$ per group) Scale bar: 40 μm. **G** and **H** Cell proliferation was assessed using the EdU assay 72 h after infection with UBE2C-overexpressing lentivirus (LV-UBE2C) of βTC-6 cells. ($N = 6$ per group) Scale bar: 40 μm. **J** and **K** Cell number was assessed using the CCK-8 48 h after si-UBE2C transfection of MIN6 (**J**) and βTC-6 cells (**K**). (N = 6–10 per group). **L** and **M** Cell number was assessed using the CCK-8 72 h after infection with UBE2C-overexpressing adenovirus (AV-UBE2C) in MIN6 (**L**) or lentivirus infection of βTC-6 cells (**M**). ($N = 6$–10 per group). **N** and **O** Representative images and proportional statistics of cell cycle distribution using PI staining in βTC-6 cells after UBE2C knockdown. ($N = 5$ per group). $^{*}P < 0.05$, $^{**}P < 0.01$, $^{***}P < 0.001$, $^{****}P < 0.0001$

genes related to β-cell maturation, such as *Slc2a2*, *G6pc2*, *Ucn3*, *Chga*, and *Ero1lb*, were less expressed in *Ube2c*^{high} subpopulation. No difference was observed in the expression of *Ins1* and *Ins2* (Fig. 1E and H). Other DEGs are presented in Supplementary Table 5. UBE2C colocalize with Ki67 and INS by immunofluorescence staining in islet sections, which confirmed the data of scRNA-seq, indicating that high-level expression of *Ube2c* is a distinct sign of proliferative β-cells (Fig. 2A).

To determine *UBE2C* expression levels in human islets, we used a recently reported dataset from non-diabetic donors [30]. Based on the annotated human β-cells, *UBE2C* was particularly expressed in a tiny population of the β-cells (Cluster-48). We defined Cluster-48 as *UBE2C*^{high} β-cells and the rest of the subpopulations as *UBE2C*^{low} β-cells (Supplementary Fig. 1A–C). Notably, proportion of G2M phase cells increased significantly in *UBE2C*^{high} β-cells group, suggesting that UBE2C is also highly expressed in proliferating human β-cells (Supplementary Fig. 1C). *UBE2C*^{high} β-cells were shown to express genes highly enriched in the cell cycle and biological processes related to ubiquitination and DNA replication by GO and KEGG analyses (Supplementary Fig. 1D–E). The cell proliferation-related genes *MKI67*, *CCNB2*, *CDK1*, *PCNA*, and *PBK*, and E3 ubiquitin ligase *CUL1* were highly expressed in *UBE2C*^{high} β-cells (Supplementary Fig. 1F). Other DEGs are presented in Supplementary Table 6. Moreover, a higher proportion of *UBE2C*^{high} β-cells was observed in human islets from obese donors (BMI ≥ 28) than in lean donors (BMI < 24) (Supplementary Fig. 1G). These results suggest that UBE2C is highly expressed in human proliferating β-cells as well as murine proliferating β-cells.

A higher expression level of UBE2C was found in islet β-cells from weaning and HFD-fed mice compared to control mice, and it promoted β-cell proliferation

Previous reports showed that islet β-cells proliferate physiologically during weaning but pathologically during the overnutrition diet. To determine whether β-cell proliferation is related to the expression level of UBE2C, we examined its protein and RNA levels in islets from CD or HFD-fed mice of different ages. The expression of UBE2C declined soon after weaning at both RNA and protein levels. Compared to CD-fed mice, the expression of UBE2C in islets from HFD-fed mice was higher (Fig. 2B–D). Immunohistochemical staining on the islets confirmed and visualized the phenomenon described above (Fig. 2E). It is worth noting that the decline of *Ube2c* expression in islets coincided with the decrease of Ki67-positive β-cells in mice with age in our previous study [21].

To determine whether *Ube2c* was related to or does regulate β-cell proliferation, knockdown and overexpression in vitro experiment were performed in two mouse β-cell lines, MIN6 and βTC-6. Cells overexpressing *Ube2c* demonstrated enhanced viability and proliferation while cells with *Ube2c* knockdown showed reduced proliferation (Fig. 2F–M). To further investigate whether reduced proliferation in *Ube2c* knockdown cells was due to cell cycle regulation, PI staining and flow cytometry analysis were performed. We found a reduced proportion of cells in the G1 phase and an increased proportion of cells in the G2/M phase in *Ube2c* knockdown βTC-6 cells compared to the control (Fig. 2N–O). Collectively, these data indicate that UBE2C promotes β-cell proliferation through self-replication based on cell cycle renewal.

Impaired insulin secretion and glucose tolerance were observed in β*Ube2c*KO mice

B-cell-specific *Ube2c* knockout mice, β*Ube2c*KO, were generated to define the in vivo function of *Ube2c* in β-cells (Supplementary Fig. 2A). The expression level of UBE2C was specifically reduced in pancreatic islets from β*Ube2c*KO mice, while it showed no significant difference in other organs or tissues, such as the liver, adipose tissue, and skeletal muscles, compared to the control mice (Supplementary Fig. 2B–C). Physiologically, *Ube2c* knockout did not alter body weight (Fig. 3A) or fasting blood glucose levels but increased 2-h postprandial blood glucose levels in juvenile mice during 4-week-old weaning (Fig. 3B). Compared to the control mice, β*Ube2c*KO mice developed glucose intolerance at 4 weeks of age and presented significantly higher plasma glucose levels during the glucose tolerance test (Fig. 3D). We further divided 4-week-old β*Ube2c*KO mice and their littermates randomly into HFD and CD groups to investigate the function of UBE2C during diabetic pathophysiology. Continuous monitoring of body weight showed increased body weight in HFD-fed mice compared with CD-fed mice; however, no significant difference was observed between β*Ube2c*KO and control mice (Fig. 3F). Different sex could exhibit divergent metabolic phenotypes [31], so we chose only male mice to do the rest of the research due to no significant increase in body weight and blood glucose level in female β*Ube2c*KO mice in HFD group compared to CD group (Fig. 3G). We found that the glucose clearance capacity of β*Ube2c*KO mice decreased significantly with prolonged HFD feeding compared to that of control mice (Fig. 3H–K). Also, pancreatic insulin concentration of βUbe2cKO mice decreased from the beginning of weaning stage to 32 weeks of age (Fig. 3L).

To determine the main cause of decreased glucose clearance capacity, insulin and glucagon secretion, and insulin sensitivity of metabolic tissues were analysed.

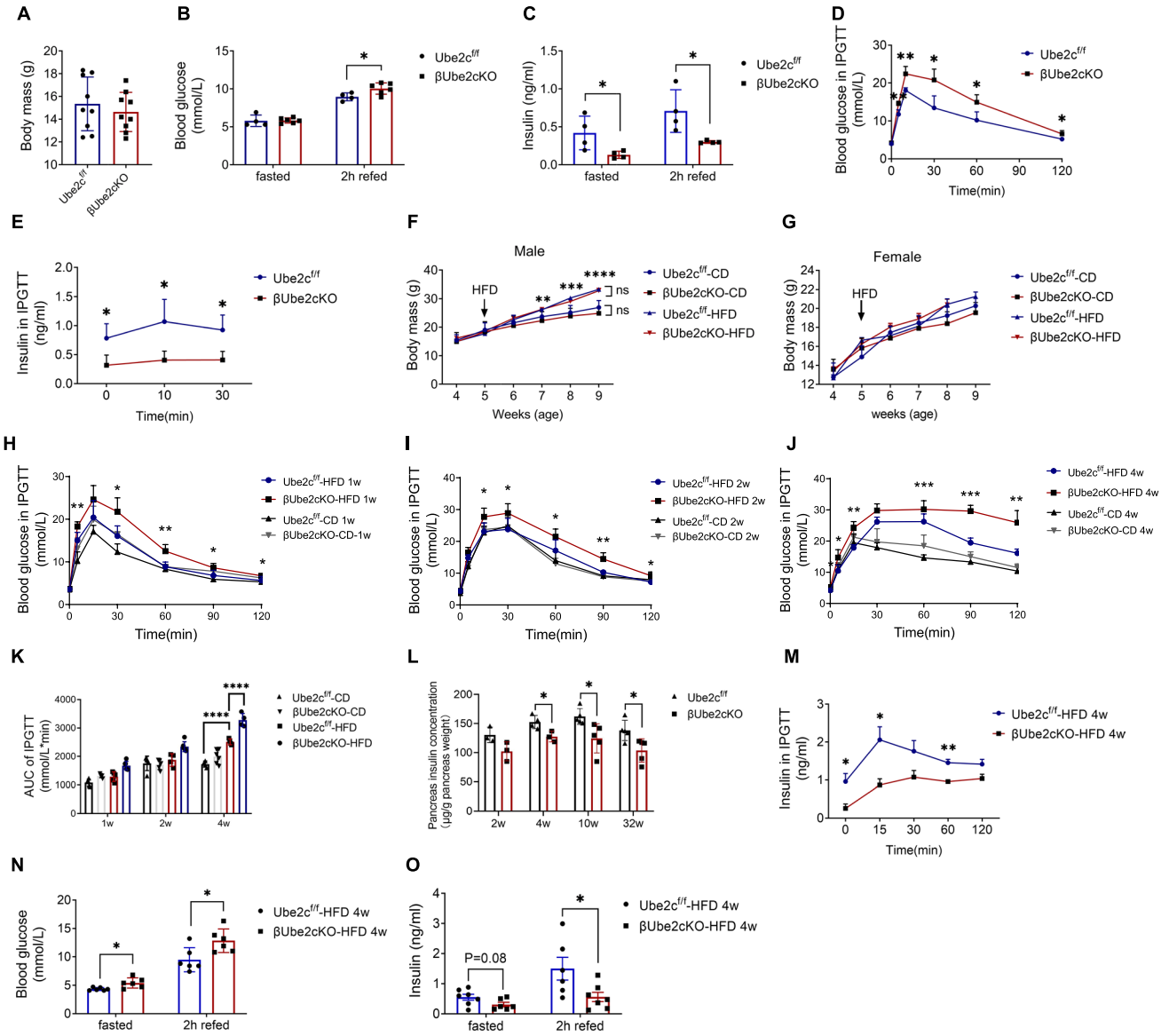

Fig. 3 Impaired glycaemic control in weaning and HFD-fed β*Ube2c*KO mice. **A** Bodyweights of 4-week-old β*Ube2c*KO male weaning mice and littermate controls. **B** and **C** Fasting blood glucose and 2-h postprandial blood glucose (**B**), and fasting insulin and 2-h postprandial insulin (**C**) levels after a 12-h overnight fasting. ($N=4$–10 mice/group). **D** and **E** Intraperitoneal glucose tolerance on 4-week-old β*Ube2c*KO weaning mice: **D** Blood glucose level during IPGTT (2 g/kg glucose), **E** Plasma insulin concentration during the IPGTT (3 g/kg glucose). ($N=4$–6 mice/group). **F**–**O** The 4-week-old β*Ube2c*KO mice and controls were randomized into normal CD and HFD feeding groups after 1 week of adaptive feeding. **F**, **G** Weekly body weight measurements of the male and female mice. **H**–**J** Blood glucose levels at 0, 5, 15, 30, 60, 90, and 120 min under IPGTT (2 g/kg glucose) at 1, 2, and 4 weeks of CD or HFD feeding from male *Ube2c*$^{f/f}$ and β*Ube2c*KO mice. **K** AUC calculation for glucose levels during the IPGTT. **L** Insulin content from male *Ube2c*$^{f/f}$ and β*Ube2c*KO mice was determined and normalized to pancreas weight at indicated time. **M** Insulin levels at 0, 15, 30, 60, and 120 min during IPGTT in the HFD group after 4 weeks of feeding. **N**, **O** Fasting for 12 h after 4 weeks of HFD feeding, blood glucose, and serum insulin levels of fasting and 2-h postprandial were measured. $N=4$–6 mice/group $^*P<0.05$, $^{**}P<0.01$

Compared to the control mice, β*Ube2c*KO mice showed impaired insulin secretion at 4 weeks old both in the fasting state or postprandially (Fig. 3C), and this phenomenon persisted in HFD feeding mice (Fig. 3N, O). However, glucagon secretion did not differ between β*Ube2c*KO and the control mice (Supplementary Fig. 4A–C). In addition, glucose-challenged insulin secretion was impaired in β*Ube2c*KO mice both weaning period and HFD feeding (Fig. 3E and M). The ITT was used to estimate whole-body insulin sensitivity, and no difference was found between the control and β*Ube2c*KO mice (Supplementary Fig. 3A–C). We also assessed insulin sensitivity in the

major insulin target organs; however, no significant change in the phosphorylated protein kinase B (p-AKT)/AKT ratio was found in β*Ube2c*KO mice compared to that in the control (Supplementary Fig. 3D–F). Collectively, these data suggest that *Ube2c* specific deletion in islet β-cells impairs insulin secretion, which contributes to hyperglycaemia in β*Ube2c*KO mice.

Decreased proliferation rate and secretory capacity of β-cells in β*Ube2c*KO mice resulted in impaired insulin secretion

To identify the factors contributing to the impaired insulin secretion in β*Ube2c*KO mice, pancreatic sections with various staining methods were used to visualize the beta cell mass and the composition of the islets in

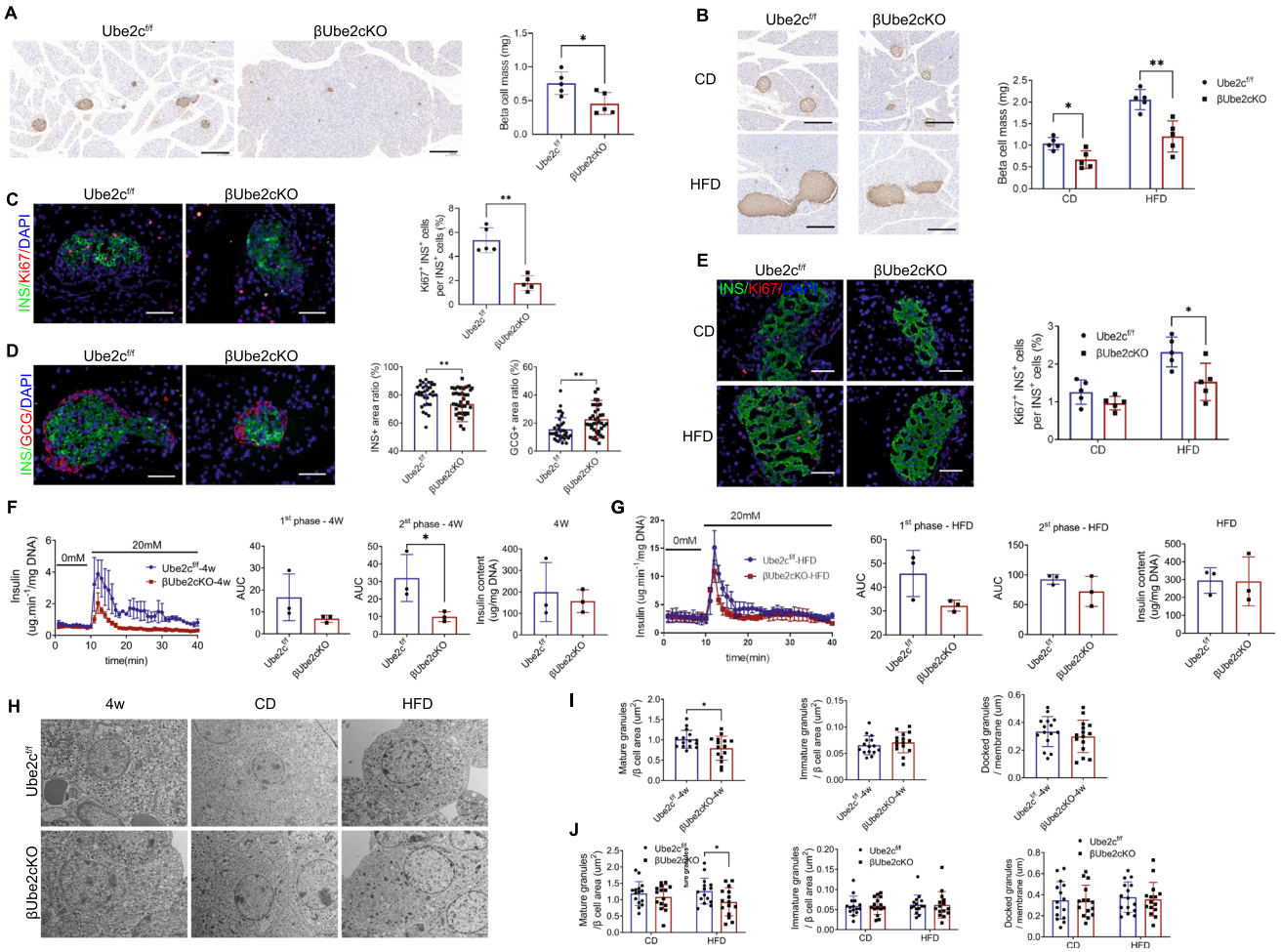

Fig. 4 β*Ube2c*KO leads to the reduced proliferative and secretory capacity of islet β-cells to promote diabetes mellitus. **A** and **B** Representative immunohistochemistry images of insulin in pancreatic sections from male β*Ube2c*KO and control mice at 4 weeks of age (**A**) or fed CD or HFD for 4 weeks (**B**) and total β-cell mass (mg) assessed as described under Methods. ($N=5$ mice/group, at least 10 islet/mouse and 1000 beta cells /mouse) Scale bar: 200 μm. **C**, **E** Representative immunofluorescence images showing Ki67$^+$ INS$^+$ cells in pancreatic sections from male β*Ube2c*KO and control mice at 4 weeks of age (**C**) or fed CD or HFD for 4 weeks (**E**) (scale bar: 40 μm). The percentage of Ki67$^+$ INS$^+$ cells in the total INS$^+$ cells is shown on the right. ($N=5$ mice/group, at least 10 islet /mouse and 1000 beta cells /mouse). **D** Representative immunofluorescence images showing double-labelling for insulin (green) and glucagon (red) on pancreatic sections from male β*Ube2c*KO and control mice at 4 weeks of age (scale bar: 40 μm). Quantification of insulin- and glucagon-stained areas is shown on the right side. ($N=8$–15 islets/mice, $N=4$–5 mice/group). **F** and **G** Perifusion assays of islets were performed in male β*Ube2c*KO mice of 4-week-old (**F**) and HFD feeding for 4 weeks (**G**). Islets were perfused with glucose (0 mM) for 0–10 min and high glucose (20 mM) for 10–40 min ($N=120$ islets/mouse, $N=3$ mice per group). First-phase insulin secretion, second-phase insulin secretion, and intracellular insulin content are shown on the right side. **H** Representative electron micrographs showing β-cells from male β*Ube2c*KO and control mice at 4-week-old (F) or after 4 weeks of CD or HFD feeding (scale bar: 2 mm). **I** and **J** Quantification of mature, immature, and docked insulin granules in β-cells of islets of male β*Ube2c*KO and control mice at 4 weeks of age (**I**) and after 4 weeks of feeding with HFD or CD (**J**) ($N=12$ β-cells/group, $N=6$–8 islets/group, $N=3$ mice/group)

β*Ube2c*KO mice. A significant reduction in islet size (cross-sectional area) (Supplementary Fig. 5A, B) and beta cell mass (Fig. 4A) of β*Ube2c*KO mice compared to the control mice had occurred by 4-week-old weaning. Moreover, islet size distribution analysis showed that the proportion of large islets decreased, while the proportion of small islets increased in β*Ube2c*KO mice compared with the control mice during CD feeding (Supplementary Fig. 5C, D). Male β*Ube2c*KO mice also had a moderate yet significant reduction in beta cell mass (Fig. 4B). The same tendency, but a more pronounced decrease in β-cell mass and islet size distribution (Fig. 4B, Supplementary Fig. 5E), was found after 4 weeks of HFD feeding in β*Ube2c*KO mice. Co-staining of insulin and glucagon was further performed to estimate the islet composition. Compared to the control mice, a smaller proportion of β-cells but a larger proportion of α cells in β*Ube2c*KO mice was observed (Fig. 4D). However, there is no difference of plasma glucagon levels in both fasting and postprandial states indicated that the relative increase in α-cell area was caused by β-cell reduction (Supplementary Fig. 4A–C). As described above, *Ube2c* was associated with β-cell replication, the proliferation indicators Ki67 and insulin were further co-stained, and the proportion of Ki67-positive β-cells remarkably decreased in β*Ube2c*KO mice during weaning or with HFD (Fig. 4C and E). These data revealed that the absence of *Ube2c* in islet β-cells reduced their proliferative capacity resulting in insufficient compensation of β-cell proliferation under metabolic stress such as weaning or a high-calorie diet.

Islet perfusion was performed on weaning mice (4 weeks old) to examine insulin secretion capacity in β*Ube2c*KO mice. After correction with the DNA mass, a significant decrease in glucose-stimulated second-phase insulin secretion was observed in β*Ube2c*KO mice compared to the control mice (Fig. 4F). However, no difference was observed in the first phase of insulin secretion and insulin content. After 4 weeks of HFD feeding, the islet perifusion results of β*Ube2c*KO mice were similar to those of weaned mice, despite no statistical differences (Fig. 4G). In vitro GSIS experiments also showed that β*Ube2c*KO mice had significantly decreased insulin secretion in both CD and HFD feeding (Supplementary Fig. 4D and G). We further detected glucose-stimulated glucagon and somatostatin secretion, and no significant difference was found between β*Ube2c*KO and control mice in either CD or HFD feeding (Supplementary Fig. 4D–I). Moreover, UBE2C overexpression in primary islets and βTC-6 cells improved GSIS when corrected based on protein levels (Supplementary Fig. 4 J–L), whereas knockdown of UBE2C in βTC-6 cells decreased GSIS. These data indicated that UBE2C positively regulates insulin secretion, except for its ability to promote β-cell proliferation.

Considering the dampened glucose-stimulated insulin secretion of the *Ube2c* knockout, TEM was used to investigate the ultrastructure of β-cells, especially insulin granules. The total number of insulin granules decreased in β*Ube2c*KO mice at 4 weeks old or after 4 weeks of HFD feeding (Fig. 4H). The reduction in mature insulin granules was the primary reason for total granule reduction, but not for immature or docked granules (Fig. 4I and J). Collectively, these data suggest that reduced β-cell mass contributes to the basal decrease in plasma insulin levels, whereas reduced mature granules contribute to glucose-stimulated insulin secretion in vivo, which finally promotes diabetes onset.

UBE2C promotes β-cell proliferation by ubiquitinating of PER1

Usually, UBE2C interacts with substrates and E3 ubiquitin ligases to ubiquitinate target proteins and degrade them through the proteasome pathway. The Cys114 site of human UBE2C protein is used to bind ubiquitin molecules. We found that human and mouse UBE2C were highly conserved; therefore, we constructed a mouse plasmid with the Cys mutation at the UBE2C114 site ($UBE2C^{C114S}$). The mouse cell line βTC-6 was transfected with WT, mutant (MT), and vector plasmids, and WB experiments revealed that $UBE2C^{C114S}$ did not affect UBE2C expression (Fig. 5A). Moreover, the CCK-8 and EdU assays showed that $UBE2C^{C114S}$ lost the capacity to promote β-cell proliferation compared to the WT plasmid (Fig. 5B–D), suggesting that the ubiquitin-binding site of UBE2C contributes to its molecular function.

To identify the possible substrate proteins and E3 binding to UBE2C, immune precipitation and MS using the UBE2C antibody were performed. Using the immunoglobulin (Ig) G control, background proteins were removed, and 296 and 317 intercalating proteins were found in LV-GFP (physiological condition) or LV-UBE2C (proliferative condition)-infected βTC-6 cells, respectively. In the physiological state, βTC-6 itself proliferates actively with high expression of UBE2C, and the high number of identified proteins (296) derived from the LV-GFP group reflects this condition. More interacting proteins (317) were identified after UBE2C overexpression, suggesting that the substrates of UBE2C in β-cells under physiological and proliferative conditions may differ. Among them, several core proteins in E3 ubiquitin ligase, including CUL1 (a member of the SCF complex), HERC2, CBLB, MID1, and members of the E1 ubiquitin

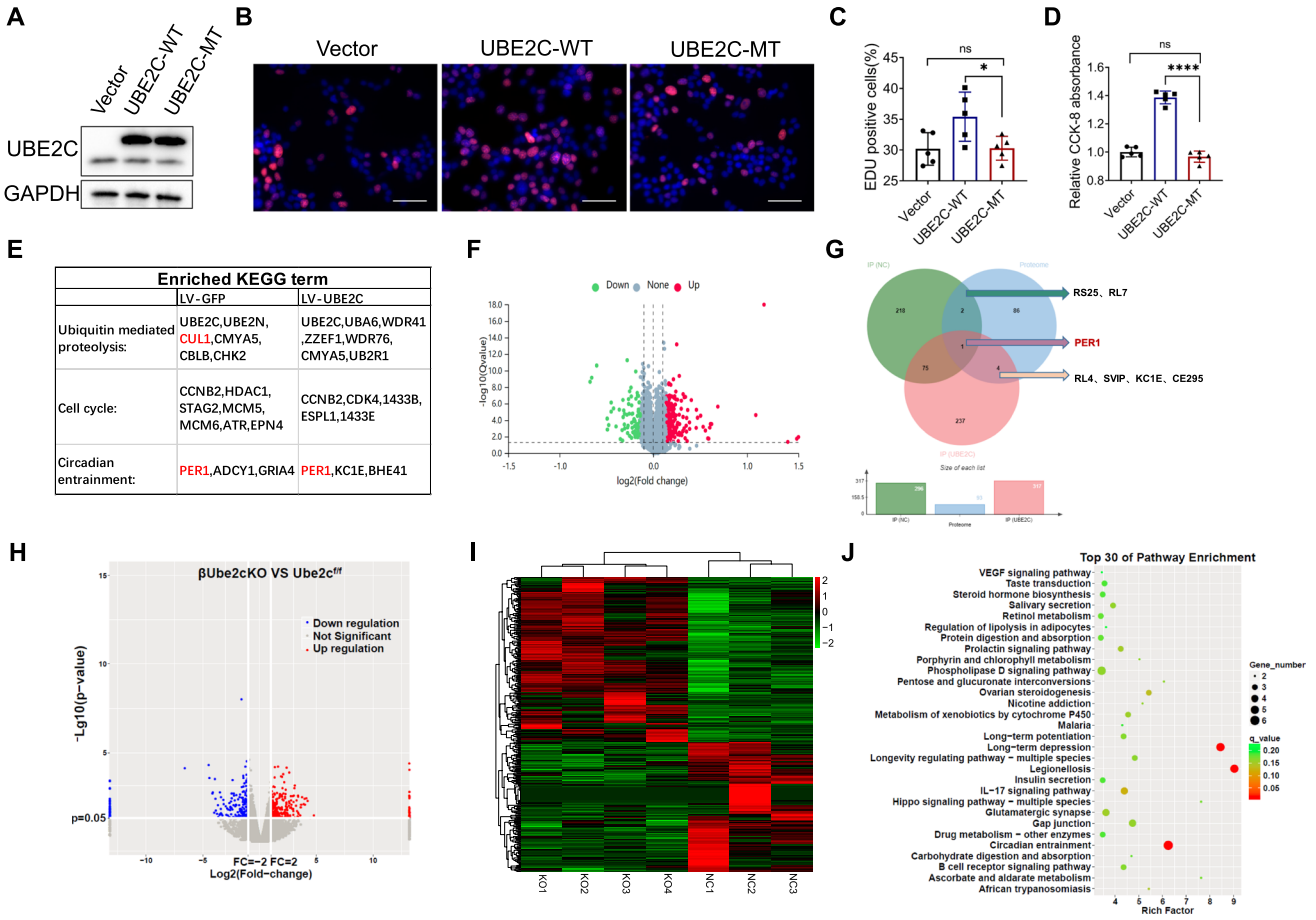

Fig. 5 Co-immunoprecipitation combined with MS and RNA-seq for the target proteins of UBE2C ubiquitination. **A**–**D** The UBE2C ubiquitin-binding site mutant plasmid of mice ($UBE2C^{C114S}$) was constructed. The vector, WT, and MT plasmids were transfected with βTC-6 cells, **A** Western blotting for UBE2C protein, **B** and **C** EdU for cell proliferation and **D** CCK-8 for cell number. ($N=5$ per group) $^{*}P<0.05$, $^{****}P<0.0001$. **E** An LV-UBE2C stably transformed βTC-6 cell line and the LV-GFP control strain were constructed. Total protein was extracted by MG132 (10 μmol/L) pretreatment for 4 h and analysed by co-immunoprecipitation and mass spectrometry with the UBE2C antibody. The KEGG database showed proteins to be enriched in "ubiquitination-mediated protein hydrolysis", "cell cycle", and "circadian entrainment" using mass spectrometry. **F** Volcano plots of differentially expressed proteins (DEPs) for LV-UBE2C vs. the negative control (LV-NC) using TMT quantification proteomics. **G** Venn diagrams of protein analysis by CO-IP mass spectrometry and downregulated DEPs from TMT quantification proteomics (LV-UBE2C vs LV-NC). **H**–**J** Extracted islets from HFD-fed β*Ube2c*KO and control mice at 4 weeks of age were subjected to RNA-seq, and DEGs were screened using |FC|> 2 and $P<0.05$. **H** and **I** Volcano plots and heatmaps of DEGs. **J** Analysis of signalling pathway enrichment of DEGs using the KEGG database

activator UBA6, were detected (Fig. 5E). Quantification TMT proteomics of βTC-6 cell lines was also performed to identify possible target proteins that were expressed at lower levels after UBE2C overexpression (Fig. 5F). Venn diagrams showed that PER1 was detected in both the control and UBE2C overexpression groups using the co-immunoprecipitation technique, and PER1 was decreased significantly after UBE2C overexpression (Fig. 5G). As ever reported that PER1 is an important negative regulator of "biological clock" that negatively regulates tumour proliferation, and the SCF complex can degrade PER1 through ubiquitination, CUL1 is the core region of the SCF complex [32, 33]. Besides, RNA-seq performed on HFD-fed control and β*Ube2c*KO mouse islets revealed that significantly expressed genes enriched in "circadian entrainment pathway" (Fig. 5H–J), which corresponds to the function of the biological clock gene Per1. Together, these data provide evidence that the UBE2C-CUL1-PER1 complex participates in β-cell proliferation.

We further proved that PER1 and CUL1 could co-precipitate using the UBE2C antibody (Fig. 6A), indicating that UBE2C interacts with PER1 and CUL1. The colocalization of UBE2C and PER1 in islet β-cells was further verified by immunofluorescence (Fig. 6E). The transcriptional level of Per1 was detected using PCR, and we found that neither Ube2c overexpression nor knockout in primary islets influenced Per1 expression (Fig. 6F). However, WB showed that PER1 expression was reduced upon

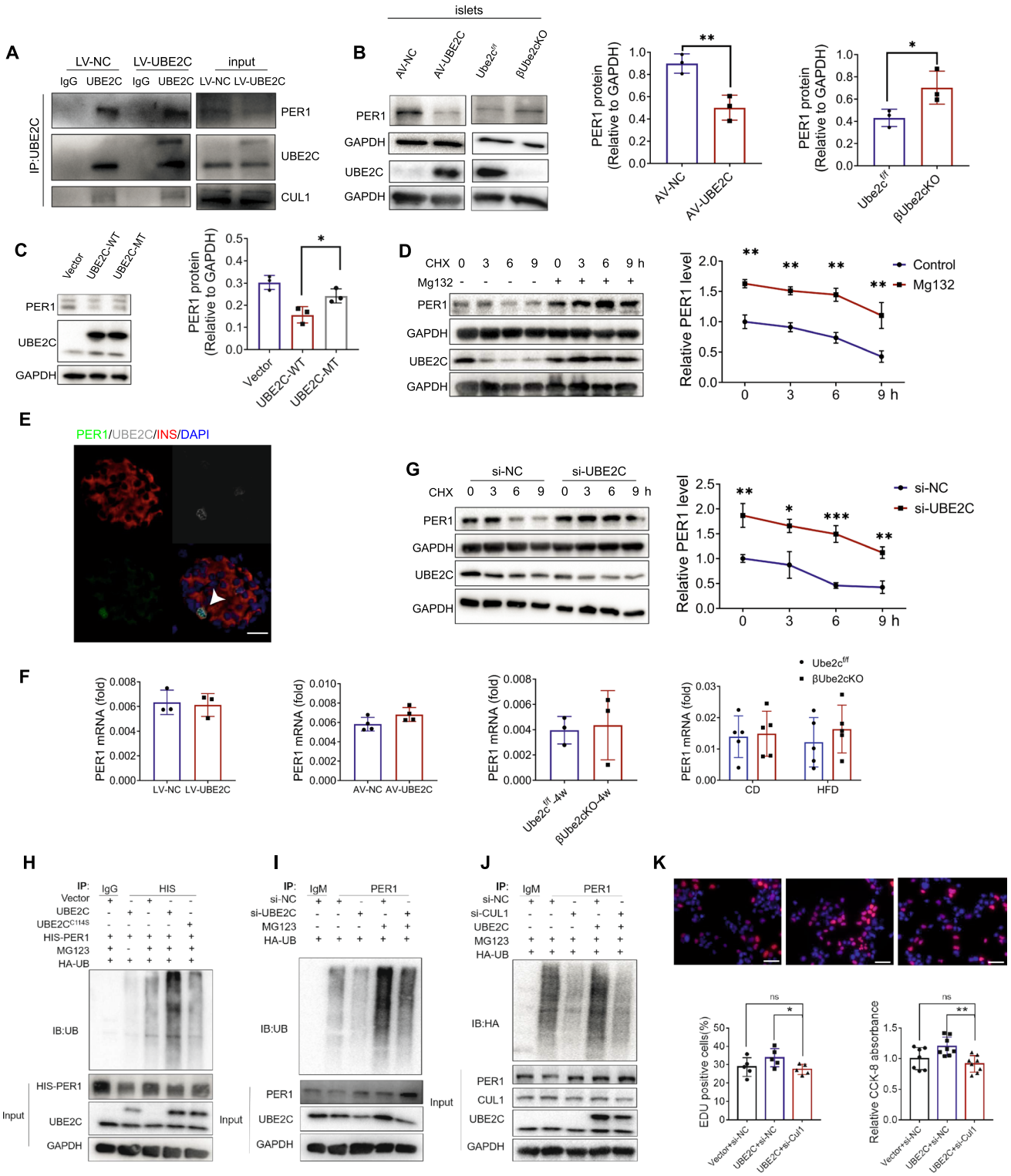
A
LV-NC
LV-UBE2C
input
IgG UBE2C IgG UBE2C LV-NC LV-UBE2C
IP:UBE2C
PER1
UBE2C
CUL1
B
islets
AV-NC
AV-UBE2C
Ube2c f/f
βUbe2cKO
PER1
GAPDH
UBE2C
GAPDH
PER1 protein (Relative to GAPDH)
C
Vector
UBE2C-WT
UBE2C-MT
D
CHX 0 3 6 9 0 3 6 9 h
Mg132 - - - - + + + +
Relative PER1 level
Control
Mg132
E
PER1/UBE2C/INS/DAPI
G
si-NC
si-UBE2C
F
PER1 mRNA (fold)
LV-NC LV-UBE2C
AV-NC AV-UBE2C
Ube2c f/f -4w
βUbe2cKO-4w
CD
HFD
H
IP: IgG HIS
Vector
UBE2C
UBE2C C114S
HIS-PER1
MG123
HA-UB
IB:UB
Input
I
IP: IgM PER1
si-NC
si-UBE2C
MG123
HA-UB
J
IP: IgM PER1
si-NC
si-CUL1
UBE2C
MG123
HA-UB
IB:HA
CUL1
K
EDU positive cells(%)
Relative CCK-8 absorbance
ns
Vector+si-NC
UBE2C+si-NC
UBE2C+si-Cul1

◂**Fig. 6** UBE2C regulates PER1 degradation by ubiquitination. **A** LV-UBE2C stably transfected βTC-6 cell line and control line were constructed. Pretreatment with MG132 (10 μmol/L) for 4 h was performed. Total protein was extracted for co-immunoprecipitation with UBE2C antibody. Protein expression of PER1, UBE2C, and CUL was measured using Western blotting. **B** Islets were overexpressed/knockout for UBE2C followed using Western blotting detection of expression of PER1 protein. Band density was measured and normalized to GAPDH ($N=3$). **C** Western blotting detection of PER1 protein expression in βTC-6 cells transfected with null, wild-type (WT), mutant (MT) UBE2C plasmids. Band density was measured and normalized to GAPDH ($N=3$). **D** Western blotting detection of protein expression of PER1 and UBE2C in βTC-6 cells treated with CHX (50 μg/mL) with or without MG132 (10 μmol/L) for 0, 3, 6, and 9 h. The rate of PER1 degradation was calculated on the right. ($N=3$). **E** Representative images of UBE2C (white), PER1 (green), INS (red), and DAPI (blue) immunostaining in the pancreas of 4-week-old C57BL/6J mice. Scale bar: 20 μm. **F** *Per1* mRNA expression in βTC-6 and islets overexpressing UBE2C; *Per1* mRNA expression in β*Ube2c*KO mice at 4 weeks of age and fed with HFD for 4 weeks in islets. ($N=3$–6 per group). **G** After treatment of βTC-6 cells with si-UBE2C and treatment with CHX (50 μg/mL) for 0, 3, 6, and 9 h before sample collection, protein expression of PER1 and UBE2C was detected using Western blotting and the rate of PER1 degradation was calculated. (N = 3). **H** HA-UB, 6*HIS-PER1, and UBE2C vector control or WT or MT overexpression plasmids were co-transfected into HEK293T cells, treated with or without MG132 for 4 h before sample collection, and PER1 ubiquitination in each group was measured using Western blotting of a ubiquitin antibody after co-immunoprecipitation with HIS-tagged antibody. **I** βTC-6 treated with si-UBE2C was transferred into HA-UB plasmids with or without MG132 treatment for 4 h before sample collection, and PER1 ubiquitination in each group was detected using Western blotting of a ubiquitin antibody after co-immunoprecipitation with PER1 antibody. **J** βTC-6 treated with si-CUL1 was transferred into HA-UB plasmids along with UBE2C plasmids or Vector plasmids, treated with MG132 for 4 h before sample collection, and PER1 ubiquitination in each group was detected using Western blotting of HA antibody after co-immunoprecipitation with PER1 antibody. **K** si-CUL1 or si-NC with vector or UBE2C overexpression plasmids were co-transfected with βTC-6 cells. EdU assay for cell proliferation and CCK-8 assay for cell number in the Vector + si-NC, UBE2C + si-NC, and UBE2C + si-CUL1 groups (scale bar: 40 μm) ($N=5$–8 per group). $^{*}P<0.05$, $^{**}P<0.01$, $^{***}P<0.001$, $^{****}P<0.0001$

UBE2C overexpression but increased in β*Ube2c*KO mice (Fig. 6B). We questioned whether UBE2C regulates PER1 expression through ubiquitination. Thus, we transfected the UBE2C WT and UBE2C^{C114S} plasmids into βTC-6 cells and found that the UBE2C^{C114S} plasmid did not cause a change in PER1 expression (Fig. 6C). The protein synthesis inhibitor cycloheximide (CHX) and proteasome inhibitor MG132 were then applied, and PER1 degradation was found to be significantly inhibited by MG132 (Fig. 6D), similar to the effect of *Ube2c* knockdown (Fig. 6G). The ubiquitination of PER1 was then detected in UBE2C WT and UBE2CC114S plasmid-overexpressing cells. UBE2C WT, but not UBE2C^{C114S}, mediated the notable increase in PER1 ubiquitination (Fig. 6H). Co-immunoprecipitation also showed that UBE2C knockdown significantly reduced PER1 ubiquitination (Fig. 6I).

To demonstrate that CUL1 as an E3 ligase is also involved in UBE2C-mediated PER1 ubiquitination, the cell proliferation and ubiquitination of PER1 were also detected after CUL1 knockdown along with UBE2C plasmids or Vector plasmids. We found that the ubiquitination level of PER1 was indeed reduced after CUL1 knockdown (Fig. 6J). Moreover, CUL1 knockdown also inhibited cell proliferation induced by UBE2C overexpression (Fig. 6K), suggesting that UBE2C and CUL1 co-participate in β-cell proliferation and achieve this through ubiquitination to degrade the target protein PER1.

PER1 inhibition rescues UBE2C knockout-induced β-cell growth inhibition both in vivo and in vitro

To verify the role of PER1 in UBE2C-induced β-cell proliferation on HFD-induced diabetes, *Ube2c*$^{f/f}$ and β*Ube2c*KO mice were transfected with either shPER1 or vehicle adeno-associated viruses (AAV) (Fig. 7A). After treatment with HFD, UBE2C knockout significantly impaired glucose tolerance and inhibited insulin secretion as determined using IPGTT (Fig. 7B–E) prior to shPER1 treatment as expected. Notably, decreased PER1 completely abolished the UBE2C knockout-induced impairment glucose tolerance and inhibited insulin secretion (Fig. 7F–I). With comparable transfection efficiency (Fig. 7J), the histological studies demonstrated that knockdown of PER1 increased the number of Ki67 and insulin co-staining cells (Fig. 7K, L), as well as the β-cell mass and islet size distribution in HFD-treated β*Ube2c*KO mice (Fig. 7Q, R, Supplementary Fig. 5H, I).

The regulatory role of UBE2C to PER1 in β-cell proliferation and insulin secretion was further confirmed in vitro. PER1 inhibition significantly rescued UBE2C knockdown-induced growth inhibition, and insulin secretion in βTC-6 cells (Fig. 7M–P). Collectively, these results indicate that UBE2C reduced PER1 expression through ubiquitin-mediated proteasomal degradation, which contributes to the proliferation and glucose-stimulated insulin secretion of β-cells.

Restored UBE2C expression promotes β-cell regeneration in streptozotocin (STZ)-induced diabetic mice

STZ-induced β-cell damage causes spontaneous β-cell regeneration in neonatal and adult rodents [34]. The neonatal beta cells are from pre-existing, surviving beta cells [35]. Therefore, it is a widely used rodent models of β-cell regeneration [36, 37]. As UBE2C promotes β-cell proliferation, we treated STZ-induced diabetic mice with massive β-cell deficiency (Fig. 8A). Low doses of STZ were injected into 4-week-old C57BL/6J mice for 5 d, and hyperglycaemia

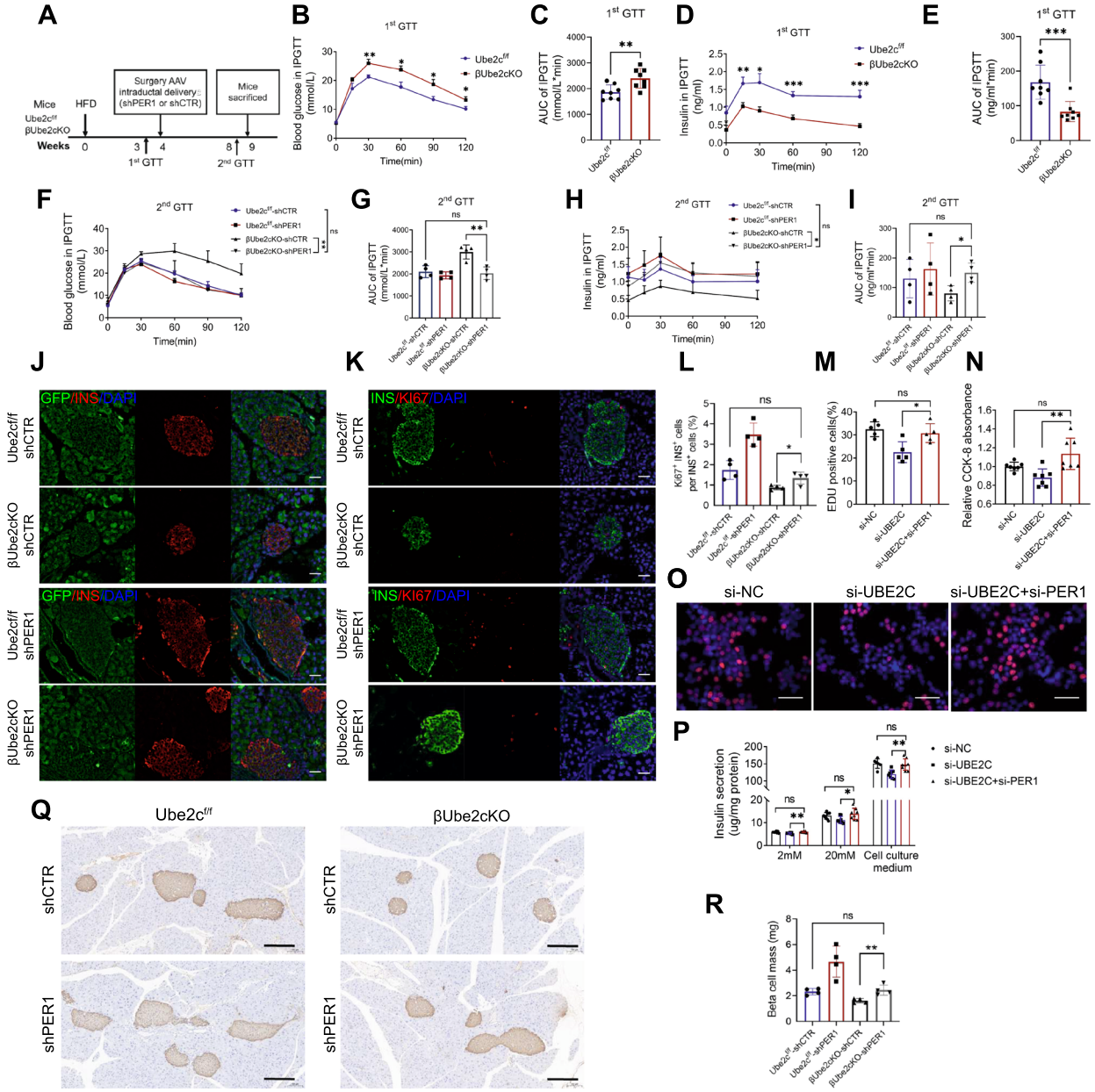

Fig. 7 PER1 inhibition rescues UBE2C knockout-induced β-cell growth inhibition. **A** Experimental procedure (schematic). **B**-**E** IPGTT glucose (**B**) and insulin release curves (**D**) and AUC of the GTT results (**C**, **E**) from male β*Ube2c*KO and *Ube2c*$^{f/f}$ mice ($N=8$ mice/group) after 3 weeks of HFD feeding. The mice were fasted overnight prior to the test (16 h). **F**-**I** After 4 weeks of high-fat feeding, the mice were randomly injected with shCTR or sh-PER1 AAV virus into the pancreatic duct ($N=4$ mice/group). Then, mice were fed for another 4 weeks after the virus treatment. IPGTT glucose (**F**) and insulin release curves (**H**) and AUC of the GTT results from each group of mice (**G**, **I**). The mice were fasted overnight prior to the test (16 h). **J** Immunofluorescence co-staining of GFP (green) and INS (red) in pancreatic sections after 5 weeks of AAV injection in the *Ube2c*$^{f/f}$ + shCTR group, the *Ube2c*$^{f/f}$ + shPER1 group, the β*Ube2c*KO + shCTR group, and the β*Ube2c*KO + shPER1 group to observe pancreatic GFP expression (scale bar: 40 μm). **K** and **L** Representative images of immunofluorescent double-stained INS (green) and Ki67 (red) (**K**) and statistical plots of Ki67 and INS double-positive cells as a percentage of total INS^{+} cells (**L**) in the *Ube2c*$^{f/f}$ + shCTR group, the *Ube2c*$^{f/f}$ + shPER1 group, the β*Ube2c*KO + shCTR group, and the β*Ube2c*KO + shPER1 group based on immunofluorescence staining (scale bar: 40 μm). ($N=4$ mice per group, at least 10 islet/mouse and 1000 beta cells/mouse).**M**-**P** si-UBE2C and si-PER1 were co-transfected with βTC-6 cells. **M**, **O** EdU assay for cell proliferation in the si-NC, si-UBE2C, and si-UBE2C + si-PER1 groups (scale bar:40 μm); **N** CCK-8 assay for cell number and **P** glucose-stimulated insulin secretion (GSIS) assay and cell culture medium with 25 mM glucose overnight for insulin secretion. ($N=7$–8 per group). **Q** and **R** Representative immunohistochemistry images of insulin (**Q**) and total β-cell mass (mg) assessed as described under Methods (**R**) (scale bar:200 μm) in the *Ube2c*$^{f/f}$ + shCTR group, the *Ube2c*$^{f/f}$ + shPER1 group, the β*Ube2c*KO + shCTR group, and the β*Ube2c*KO + shPER1 group. ($N=4$ mice per group, at least 10 islet/mouse and 1000 beta cells/mouse). $^{*}P<0.05$, $^{**}P<0.01$, $^{***}P<0.001$, $^{****}P<0.0001$

was monitored 1 month before virus injection (Fig. 8E, F). Supplementary Fig. 5J showed the β-cell deficiency changes after STZ treatment. *Ube2c*-overexpressing and control lentiviruses were injected into the pancreatic duct at 8 weeks old. Two weeks post-injection, the UBE2C-restored mice began to show a decrease in blood glucose levels and an increase in insulin levels (Fig. 8G–J). Moreover, pancreatic insulin concentration increased significantly after *Ube2c* overexpression treatment (Fig. 8L).

With decreasing glucose levels, the body weight of UBE2C-restored mice increase gradually compared to that of the control mice (Fig. 8B). Glucose tolerance was also partially improved in *Ube2c*-restored mice owing to the increased glucose-stimulated insulin secretion in vivo (Fig. 8C and D). However, glucagon levels were not different between the groups (Fig. 8K), suggesting a specific effect of UBE2C on β-cells.

The co-staining of GFP and insulin showed that the lentivirus infects the entire pancreas and islets in both STZ-LV-NC and STZ-LV-UBE2C groups (Fig. 8M). Interestingly, co-staining of Ki67 and insulin showed an increased proliferation rate of β-cell from Ube2c-restored mice (Fig. 8N), which improved the proportion of β-cells to α-cells (Fig. 8O), and partially recovered beta cell mass and islet size terminally (Fig. 8P, Supplementary Fig. 5F, G). These data indicate the molecular function of UBE2C in β-cell proliferation and show its application prospects in diabetic patients with β-cell deficiency.

Discussion

We identified a vigorously proliferating subtype of β-cells, the highly expressed ubiquitin-binding enzyme UBE2C, which binds to the ubiquitin ligase CUL1 and jointly recognizes the target protein PER1 to activate β-cell replication. The increased UBE2C promotes PER1 degradation through the ubiquitinated proteasome degradation pathway; then the blocked cell cycle begins to renew. Our investigation extended the previous mechanistic study of the NKX6.1/UBE2C axis in β-cell replication. Moreover, our results supported that regenerated β-cells can secrete insulin adaptive to blood glucose fluctuations, suggesting a better treatment compared to insulin injection.

Human and mouse pancreatic β-cells are heterogeneous which could reflect fixed subpopulations with distinct cell cycle and functional states [26, 38]. The proportion of β-cells with proliferation capacity is nearly 1% in both adult human and murine islets but increases significantly in infants or in the initial stage in adults with chronic fuel surfeit [10–12]. Single-cell RNA sequencing (scRNA-seq) has emerged as a powerful approach to explore intercellular heterogeneity. Due to the heterogeneity of β-cells, proliferation is only carried out in a small group of β-cells in adult, not all β-cells. Our investigation using bioinformatics and β*Ube2c*KO mice proved that UBE2C could be a signature gene of the proliferative subgroup. *Ube2c*^{high} β-cell subpopulation represents β-cell under replication at that time point. β-cell replication is an instantaneous process but the resulting enlargement of islets is a cumulative process. It could be the reason why UBE2C exert significant influence the size of islets.β-cells with vigorous proliferation capacity were typically considered to have a weaker GSIS function and a lower maturity [39, 40]. In addition, genes associated with β-cell function, such as *Slc2a2*, *G6pc2*, *Ucn3*, *Chga*, and *Ero1lb*, were found to be slightly decreased, suggesting a relatively immature of these cells. However, β*Ube2c*KO mice showed impaired GSIS either in vivo or ex vivo, indicating the essential role of UBE2C in GSIS function maintenance. Although we did not reveal the detailed mechanism of impaired insulin secretion, a recent study showed that PBK kinase-inactivated mice had a significant decrease in beta cell proliferation and insulin secretion, whereas *Pbk* was found to be highly co-expressed with *Ube2c* in the subgroup of vigorously proliferating β-cells identified by us, which supports the plausibility of this phenomenon in β*Ube2c*KO mice [41]. We speculate that marker genes with high expression in proliferating β-cells may play similar functions as a functional population.

UBE2C has been reported to mostly bind to the APC/C complex to promote target protein degradation [42]; however, more than 600 types of E3 ubiquitin ligases have been found [43], and the details downstream of NKX6.1/UBE2C were elusive. Using a co-immunoprecipitation assay, our present study speculated that several targets of UBE2C, except for the APC/C complex, among which CUL1, the core subunit of the SCF complex, has been reported to participate in ubiquitination degradation as E3 ubiquitin ligase [44, 45].

The biological clock system regulates the circadian clock as well as the cell cycle system, leading to regular mitosis and rhythmic DNA replication physiologically [46–49]. In circadian clock regulation, PER1 and PER2 combine CRY1 and CRY2, respectively, to inhibit CLOCK-BMAL1 activation [50]. As a negative regulator of cell division, PER1 also interacts with the cell cycle checkpoint proteins ATM/ATR and CHK1/2 [32]. Our co-immunoprecipitation and MS analyses identified PER1 as a target of the UBE2C/CUL1 complex. It has been reported that β*Bmal1*KO mice exacerbated the progression of HFD-induced diabetes, as manifested by poor glucose tolerance and impaired beta cell proliferation [51], which was similar to our observations in β*Ube2c*KO mice. β-cell-specific *Per2* knockout mice showed alleviated glucose tolerance, in contrast to *bmal1* knockout mice [51–53]. Consistent with our finding that PER1 inhibition rescues UBE2C knockout-induced β-cell growth

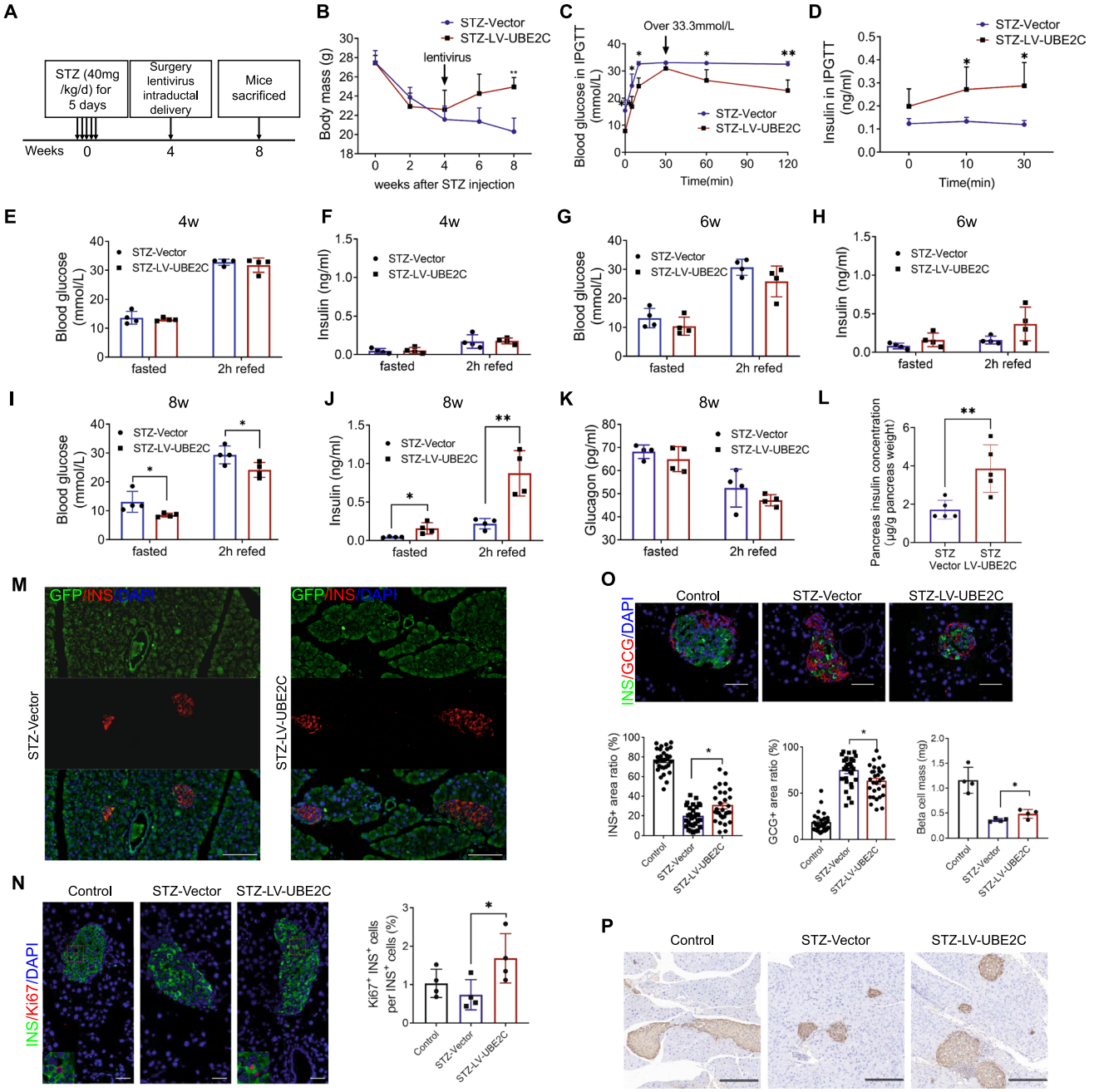

Fig. 8 UBE2C promotes islet β-cell regeneration in STZ-induced DM mice. **A** Experimental procedure (schematic). **B** Bodyweights of UBE2C-overexpressing and control mice were measured weekly after STZ injection. $N=4$ mice/group. **C**, **D** IPGTT glucose and insulin release curves 4 weeks after in situ injection within pancreatic ducts. $N=4$ mice/group. **E**–**J** Blood glucose and serum insulin levels before (**E**, **F**), 2 weeks (**G**, **H**), and 4 weeks (**I**, **J**) post-injection (corresponding to 4, 6, and 8 weeks after STZ modelling) fasting, and 2 h after resumption of feeding in the pancreatic ducts before in situ injection of UBE2C lentivirus. **K** Serum glucagon levels 4 weeks after in situ pancreatic duct injection, fasting, and 2 h after meal consumption; $N=4$ mice/group, $^{*}P<0.05$, $^{**}P<0.01$. **L** Insulin content from STZ-LV-NC and STZ-LV-UBE2C group was determined and normalized to pancreas weight. **M** Immunofluorescence co-staining of GFP (green) and INS (red) in pancreatic sections after 4 weeks of treatment to observe pancreatic GFP expression (scale bar:40 μm). **N** Representative images of immunofluorescent double-stained INS (green) and Ki67 (red) and statistical plots of Ki67 and INS double-positive cells as a percentage of total INS^{+} cells in normal C57BL/6 J mice, the STZ Vector group, and the STZ-LV-UBE2C group based on immunofluorescence staining (scale bar: 40 μm). ($N=4$ mice per group, at least 10 islet/mouse and 1000 beta cells/mouse). **O** Immunofluorescence double-stained INS (green) and GCG (red) islets and area values showing the percentage of insulin and glucagon positivity in islets (scale bar:40 μm); ($N\geq 30$ islets/group, $N=4$ mice/group). **P** Representative immunohistochemistry images of β-cells and total β-cell mass (mg) assessed as described under Methods (scale bar: 200 μm). ($N=4$ mice per group, at least 10 islet/mouse and 1000 beta cells/mouse). $^{*}P<0.05$, $^{**}P<0.01$, $^{***}P<0.001$, $^{****}P<0.0001$

inhibition both in vivo and in vitro, these data suggest that PER1, as a negative regulatory molecule of BMAL1 in β-cells, may also be involved in compensatory proliferation and insulin secretion.

Streptozocin (STZ) can be used to cause extensive damage to endogenous β-cells and induce hyperglycaemia and diabetes. STZ-induced β-cell damage causes spontaneous β-cell regeneration in neonatal and adult rodents [34]. The neonatal beta cells are all from pre-existing, surviving beta cells [35]. Therefore, it is a classical rodent models of β-cell regeneration and is widely used in multiple studies [36, 37]. Our study showed that UBE2C-induced β-cell replication was efficient in β-cell restoration. In addition, anti-apoptotic effects were observed in UBE2C highly expressed tumour cells [19]. Therefore, the molecular function of UBE2C in β-cell restoration requires further investigation.

Despite the explored mechanism of UBE2C in β-cell replication, our study had some limitations. First, NKX6.1 was reported to be the up-regulator of *Ube2c* transcription, whereas NKX6.1 was highly expressed in β-cell lifelong but not UBE2C, suggesting that the regulatory mechanism may be different between weaning and high-fat feeding. Therefore, it was predicted by IPA (data not shown) that upstream transcription factors SMAD3 and TP53 were activated in β*Ube2c*KO mice. Both SMAD3 and TP53 reported to negatively regulated beta cell proliferation [54, 55]. Also, according to our previous study [21], the expression of both Smad3 and Tp53 decreased after high-fat feeding. We speculated that both TP53 and SMAD3 may be negative regulators upstream of UBE2C, but further experimental proof is needed. Additionally, further studies should be performed to determine the specific molecular mechanisms of UBE2C knockout-induced decline in beta insulin secretion and their relationship with PBK.

In summary, we found that the conditional highly expressed gene "*Ube2c*" is a signature of vigorous replicating β-cells. UBE2C positively regulates β-cell compensatory proliferation by promoting ubiquitination and degradation of the biological clock suppressor PER1. The mechanism of UBE2C in promoting β-cells replication was used to treat STZ-induced diabetes in mice. Generally, the beneficial effect of UBE2C on islet β-cell regeneration suggests a promising application in treating diabetic patients with β-cell deficiency.

Supplementary Information The online version contains supplementary material available at https://doi.org/10.1007/s00018-023-04868-8.

Acknowledgements The authors wish to thank all research staff in Department of Endocrinology of the First Affiliated Hospital of Nanjing Medical University who participated in this work. They would like to thank the Core Facility of the First Affiliated Hospital of Nanjing Medical University for its help in the experiment. They would like to thank Professor Hongxing Fu from Shulan (Hangzhou) Hospital Affiliated to Zhejiang Shuren University Shulan International Medical College for providing the human pancreas slice samples.

Author contributions QF and TY directed the study and were responsible for study design and overall project management. HJ, SZ, YQ and YZ performed statistical analyses, participated in study design, and drafted the manuscript. HD, YL, YZ, YH, JZ, ZX, and RG analysed the data. HL, WB, and KX contributed to conception, design, and interpretation of this work. All the authors approved the final manuscript.

Funding This work was supported by the National Natural Science Foundation of China (81830023, 82070803 and 82100837).

Data availability The scRNA-seq analysis datasets during the current study are available in the Gene Expression Omnibus (GEO) repository under the accession number GSE203376 (mouse) and GSE148073 (human). Other datasets are available from the corresponding author upon reasonable request.

Declarations

Conflict of interest The authors declare no competing financial interests.

Ethical approval Animal use procedures were approved (IACUC1804001) by the Medicine Animal Care Committee of Nanjing Medical University. Experiments were conducted in accordance with relevant institutional guidelines and regulations.

Consent for publication All the authors read and approved the submission and final publication.

References

1. Sims EK, Carr ALJ, Oram RA, DiMeglio LA, Evans-Molina C (2021) 100 years of insulin: celebrating the past, present and future of diabetes therapy. Nat Med 27(7):1154–1164. https://doi.org/10.1038/s41591-021-01418-2
2. Mathieu C, Martens PJ, Vangoitsenhoven R (2021) One hundred years of insulin therapy. Nat Rev Endocrinol 17(12):715–725. https://doi.org/10.1038/s41574-021-00542-w
3. Eizirik DL, Pasquali L, Cnop M (2020) Pancreatic Î2-cells in type 1 and type 2 diabetes mellitus: different pathways to failure. Nat Rev Endocrinol 16(7):349–362. https://doi.org/10.1038/s41574-020-0355-7
4. Hudish LI, Reusch JE, Sussel L (2019) Î^2 Cell dysfunction during progression of metabolic syndrome to type 2 diabetes. J Clin Investig 129(10):4001–4008. https://doi.org/10.1172/jci129188
5. Halban PA, Polonsky KS, Bowden DW et al (2014) Î^2-cell failure in type 2 diabetes: postulated mechanisms and prospects for prevention and treatment. Diabetes Care 37(6):1751–1758. https://doi.org/10.2337/dc14-0396
6. Samnegård B, Jacobson SH, Jaremko G, Johansson BL, Sjöquist M (2001) Effects of C-peptide on glomerular and renal size and renal function in diabetic rats. Kidney Int 60(4):1258–1265. https://doi.org/10.1046/j.1523-1755.2001.00964.x
7. Al-Rasheed NM, Willars GB, Brunskill NJ (2006) C-peptide signals via Galpha i to protect against TNF-α-mediated apoptosis of opossum kidney proximal tubular cells. J Am Soc Nephrol 17(4):986–995. https://doi.org/10.1681/asn.2005080797

8. Li J, Zhang Y, Ye Y et al (2021) Pancreatic Î[2] cells control glucose homeostasis via the secretion of exosomal miR-29 family. J Extracell Vesicles 10(3):e12055. https://doi.org/10.1002/jev2.12055
9. Poy MN, Hausser J, Trajkovski M et al (2009) miR-375 maintains normal pancreatic alpha- and beta-cell mass. Proc Natl Acad Sci USA 106(14):5813–5818. https://doi.org/10.1073/pnas.0810550106
10. Dor Y, Brown J, Martinez OI, Melton DA (2004) Adult pancreatic β-cells are formed by self-duplication rather than stem-cell differentiation. Nature 429(6987):41–46
11. Parsons JA, Brelje TC, Sorenson RL (1992) Adaptation of islets of Langerhans to pregnancy: increased islet cell proliferation and insulin secretion correlates with the onset of placental lactogen secretion. Endocrinology 130(3):1459–1466
12. Klöppel G, Löhr M, Habich K, Oberholzer M, Heitz PU (1985) Islet pathology and the pathogenesis of type 1 and type 2 diabetes mellitus revisited. Surv Synth Pathol Res 4(2):110–125
13. Sorenson RL, Brelje TC (1997) Adaptation of islets of Langerhans to pregnancy: beta-cell growth, enhanced insulin secretion and the role of lactogenic hormones. Horm Metab Res 29(6):301–307. https://doi.org/10.1055/s-2007-979040
14. Hu FB, Manson JE, Stampfer MJ et al (2001) Diet, lifestyle, and the risk of type 2 diabetes mellitus in women. N Engl J Med 345(11):790–797. https://doi.org/10.1056/NEJMoa010492
15. Stott NL, Marino JS (2020) High fat rodent models of type 2 diabetes: from rodent to human. Nutrients. https://doi.org/10.3390/nu12123650
16. Hudish LI, Reusch J, Sussel L (2019) β Cell dysfunction during progression of metabolic syndrome to type 2 diabetes. J Clin Investig 129(10):4001–4008
17. Avrahami D, Klochendler A, Dor Y, Glaser B (2017) Beta cell heterogeneity: an evolving concept. Diabetologia 60(8):1363–1369
18. Liu PF, Chen CF, Shu CW et al (2020) UBE2C is a potential biomarker for tumorigenesis and prognosis in tongue squamous cell carcinoma. Diagnostics (Basel). https://doi.org/10.3390/diagnostics10090674
19. Chiang AJ, Li CJ, Tsui KH, Chang C, Sheu JC (2020) UBE2C drives human cervical cancer progression and is positively modulated by mTOR. Biomolecules 11(1):37
20. Tessem JS, Moss LG, Chao LC et al (2014) Nkx6.1 regulates islet β-cell proliferation via Nr4a1 and Nr4a3 nuclear receptors. Proc Natl Acad Sci USA 111(14):5242–5247. https://doi.org/10.1073/pnas.1320953111
21. Gao R, Fu Q, Jiang HM et al (2021) Temporal metabolic and transcriptomic characteristics crossing islets and liver reveal dynamic pathophysiology in diet-induced diabetes. iScience 24(4):102265. https://doi.org/10.1016/j.isci.2021.102265
22. Xiao X, Guo P, Prasadan K et al (2014) Pancreatic cell tracing, lineage tagging and targeted genetic manipulations in multiple cell types using pancreatic ductal infusion of adeno-associated viral vectors and/or cell-tagging dyes. Nat Protoc 9(12):2719–2724. https://doi.org/10.1038/nprot.2014.183
23. Wu T, Zhang S, Xu J et al (2020) HRD1, an important player in pancreatic β-cell failure and therapeutic target for type 2 diabetic mice. Diabetes 69(5):940–953. https://doi.org/10.2337/db19-1060
24. Pagala VR, High AA, Wang X et al (2015) Quantitative protein analysis by mass spectrometry. Methods Mol Biol (Clifton, NJ) 1278:281–305. https://doi.org/10.1007/978-1-4939-2425-7_17
25. Gao R, Fu Q, Jiang HM et al (2021) Temporal metabolic characteristics and transcriptomic landscape of islets and liver reveal dynamic pathophysiology and interorgan crosstalk in high-fat diet-induced diabetes. iScience 24(4):102265
26. Fu Q, Jiang H, Qian Y et al (2023) Single-cell RNA sequencing combined with single-cell proteomics identifies the metabolic adaptation of islet cell subpopulations to high-fat diet in mice. Diabetologia 66(4):724–740. https://doi.org/10.1007/s00125-022-05849-5
27. Kobak D, Berens P (2019) The art of using t-SNE for single-cell transcriptomics. Nat Commun 10(1):5416. https://doi.org/10.1038/s41467-019-13056-x
28. Subelj L, Bajec M (2011) Unfolding communities in large complex networks: combining defensive and offensive label propagation for core extraction. Phys Rev E Stat Nonlin Soft Matter Phys 83(3 Pt 2):036103. https://doi.org/10.1103/PhysRevE.83.036103
29. Fu Q, Jiang H, Qian Y et al (2022) Single-cell RNA sequencing combined with single-cell proteomics identifies the metabolic adaptation of islet cell subpopulations to high-fat diet in mice. Diabetologia 66(4):724–740
30. Fasolino M, Schwartz GW, Patil AR et al (2022) Single-cell multi-omics analysis of human pancreatic islets reveals novel cellular states in type 1 diabetes. Nat Metab 4(2):284–299. https://doi.org/10.1038/s42255-022-00531-x
31. Oraha J, Enriquez RF, Herzog H, Lee NJ (2022) Sex-specific changes in metabolism during the transition from chow to high-fat diet feeding are abolished in response to dieting in C57BL/6J mice. Int J Obes (2005) 46(10):1749–1758. https://doi.org/10.1038/s41366-022-01174-4
32. Gery S, Komatsu N, Baldjyan L, Yu A, Koeffler HP (2006) The circadian gene Per1 plays an important role in cell growth and DNA damage control in human cancer cells. Mol Cell 22(3):375–382
33. Shirogane T, Jin J, Ang XL, Harper JW (2005) SCFβ-TRCP controls clock-dependent transcription via casein kinase 1-dependent degradation of the mammalian period-1 (Per1) proteinm. Jbiolchem 280(29):26863
34. Zhong F, Jiang Y (2019) Endogenous pancreatic β cell regeneration: a potential strategy for the recovery of β cell deficiency in diabetes. Front Endocrinol 10:101. https://doi.org/10.3389/fendo.2019.00101
35. Zhao H, Huang X, Liu Z et al (2021) Pre-existing beta cells but not progenitors contribute to new beta cells in the adult pancreas. Nat Metab 3(3):352–365. https://doi.org/10.1038/s42255-021-00364-0
36. Feng Y, Qiu WL, Yu XX et al (2020) Characterizing pancreatic β-cell heterogeneity in the streptozotocin model by single-cell transcriptomic analysis. Mol Metab 37:100982. https://doi.org/10.1016/j.molmet.2020.100982
37. Tschen SI, Dhawan S, Gurlo T, Bhushan A (2009) Age-dependent decline in beta-cell proliferation restricts the capacity of beta-cell regeneration in mice. Diabetes 58(6):1312–1320. https://doi.org/10.2337/db08-1651
38. Dorrell C, Schug J, Canaday PS et al (2016) Human islets contain four distinct subtypes of β cells. Nat Commun 7:11756. https://doi.org/10.1038/ncomms11756
39. Klochendler A, Caspi I, Corem N et al (2016) The genetic program of pancreatic β-cell replication in vivo. Diabetes 65(7):2081–2093
40. Ruijtenberg S, Sander VDH (2016) Coordinating cell proliferation and differentiation: antagonism between cell cycle regulators and cell type-specific gene expression. Cell Cycle 15(2):196–212
41. Ma J, Xing B, Cao Y et al (2021) Menin-regulated Pbk controls high fat diet-induced compensatory beta cell proliferation. EMBO Mol Med 13(5):e13524. https://doi.org/10.1525/emmm.202013524
42. Ben-Eliezer I, Pomerantz Y, Galiani D, Nevo N, Dekel N (2015) Appropriate expression of Ube2C and Ube2S controls the progression of the first meiotic division. FASEB J 29(11):4670–4681. https://doi.org/10.1096/fj.15-274522

43. Ye Y, Rape M (2009) Building ubiquitin chains: E2 enzymes at work. Nat Rev Mol Cell Biol 10(11):755–764. https://doi.org/10.1038/nrm2780
44. Xie J, Jin Y, Wang G (2019) The role of SCF ubiquitin-ligase complex at the beginning of life. Reprod Biol Endocrinol 17(1):101. https://doi.org/10.1186/s12958-019-0547-y
45. Shirogane T, Jin J, Ang XL, Harper JW (2005) SCFbeta-TRCP controls clock-dependent transcription via casein kinase 1-dependent degradation of the mammalian period-1 (Per1) protein. J Biol Chem 280(29):26863–26872. https://doi.org/10.1074/jbc.M502862200
46. Reppert SM, Weaver DR (2001) Molecular analysis of mammalian circadian rhythms. Annu Rev Physiol 63(1):647
47. Yagita K (2001) Molecular mechanisms of the biological clock in cultured fibroblasts. Science 292(5515):278–281
48. Farshadi E, van der Horst GTJ, Chaves I (2020) Molecular links between the circadian clock and the cell cycle. J Mol Biol 432(12):3515–3524. https://doi.org/10.1016/j.jmb.2020.04.003
49. Takahashi JS (2017) Transcriptional architecture of the mammalian circadian clock. Nat Rev Genet 18(3):164–179. https://doi.org/10.1038/nrg.2016.150
50. Ko CH, Takahashi JS (2006) Molecular components of the mammalian circadian clock. Hum Mol Genet 15(Spec No 2):R271–R277. https://doi.org/10.1093/hmg/ddl207
51. Rakshit K, Hsu TW, Matveyenko AV (2016) Bmal1 is required for beta cell compensatory expansion, survival and metabolic adaptation to diet-induced obesity in mice. Diabetologia 59(4):734–743. https://doi.org/10.1007/s00125-015-3859-2
52. Marcheva B, Ramsey KM, Buhr ED et al (2010) Disruption of the clock components CLOCK and BMAL1 leads to hypoinsulinaemia and diabetes. Nature 466(7306):627–631. https://doi.org/10.1038/nature09253
53. Zhao Y, Zhang Y, Zhou M, Wang S, Hua Z, Zhang J (2012) Loss of mPer2 increases plasma insulin levels by enhanced glucose-stimulated insulin secretion and impaired insulin clearance in mice. FEBS Lett 586(9):1306–1311. https://doi.org/10.1016/j.febslet.2012.03.034
54. Wang HL, Wei B, He HJ et al (2022) Smad3 deficiency improves islet-based therapy for diabetes and diabetic kidney injury by promoting β cell proliferation via the E2F3-dependent mechanism. Theranostics 12(1):379–395. https://doi.org/10.7150/thno.67034
55. Hoshino A, Ariyoshi M, Okawa Y et al (2014) Inhibition of p53 preserves Parkin-mediated mitophagy and pancreatic β-cell function in diabetes. Proc Natl Acad Sci USA 111(8):3116–3121. https://doi.org/10.1073/pnas.1318951111